Front-curvature effects in the dynamics of confined radiatively bistable plasmas: Perfect patterns and Ostwald ripening

Igor Aranson
Department of Physics, Bar-Ilan University, Ramat Gan 52900, Israel

Baruch Meerson
Racah Institute of Physics, Hebrew University of Jerusalem, Jerusalem 91904, Israel

Pavel V. Sasorov
Institute of Theoretical and Experimental Physics, Moscow 117259, Russia
(Received 24 August 1994)

Front-curvature effects in the dynamics of a confined optically thin isotropic plasma, which is heated by an external energy source and cools radiatively, are investigated under conditions of thermal bistability. Reduced governing equations for such a plasma are derived, based on the elimination of the acoustic modes. Possible large-scale equilibria, describing segregation of the plasma into two "phases," dense and cool, and rarefied and hot, are found. Only objects with a constant mean curvature of their boundaries (the simplest of these are slabs, cylinders, and spheres) are shown to represent such equilibria. The curvature introduces a small correction to the "area rule" value of the equilibrium plasma pressure. The governing equations are reduced further and employed for stability analysis of individual equilibrium objects and of their ensembles. An equilibrium slab is found to be stable with respect to arbitrary perturbations. Similarly, a circular or spherical "drop" (or "bubble") is stable with respect to deformations of their shape. On the contrary, the same drop or bubble can be unstable with respect to a purely radial mode, and stability arguments determine the minimum possible radius of these objects. Ensembles of drops or bubbles show strong background-mediated competition (Ostwald ripening). Possible self-similar asymptotics of the time-dependent distribution of a large number of drops with respect to their radii are found. Two-dimensional numerical simulations of the dynamics of a confined bistable plasma are performed in a square "box". When starting from a broadband noise perturbation around a uniform state, we observe radiative segregation of the plasma, followed by background-mediated competition and establishment of either the slab-type, or the drop (or bubble)-type equilibrium. Finally, deformation instability of planar "evaporation" fronts, similar to the Darrieus-Landau instability of the laminar flame propagation, is found.

PACS number(s): 52.35.Py, 47.70.Mc, 47.54.+r, 95.30.Qd

I. INTRODUCTION

Thermal bistability of optically thin plasmas, which are subject to some heating and cool radiatively, have attracted considerable attention, mainly because of astrophysical applications [1]. Thermal bistability manifests itself in segregation of the plasma into two locally stable phases (cool and dense, and hot and rarefied). Radiative condensation instability (RCI), first considered by Field [2], is intrinsically related to thermal bistability. The RCI is believed to play an important role in the development of such diverse plasma objects as interstellar [1] and intergalactic [3] clouds, solar prominences [4], so called "marfes" in tokamaks [5], and radiative Z pinches [6]. A large number of works was devoted to various aspects of the dynamics of the RCI, starting from the comprehensive linear theory by Field [2]. The nonlinear theory of the RCI has attracted much recent attention in the context of self-organization and pattern formation in optically thin radiating plasmas [7–14].

Most of the nonlinear studies of radiative bistability and RCI were limited to the one-dimensional (planar) geometry, although two-dimensional dynamics was addressed numerically in the context of solar physics [15]. Essentially one-dimensional dynamics is often realized in strongly magnetized, low-β plasmas, where the magnetic field suppresses both transverse plasma motions and transverse heat conduction. (Here β is the ratio of the plasma pressure p to the magnetic pressure $B^2/8\pi$.) A possible example of such systems is provided by the coronal plasma loops in the solar atmosphere [16]. In contrast, in the interstellar and intergalactic plasmas, the magnetic fields are often insufficient to strongly magnetize the plasma [17], so that the dynamics of the RCI in such plasmas is in general three dimensional.

In weak magnetic fields (or for a low degree of plasma ionization), the values of the plasma heat conduction along and across the field are comparable, so that, for simplicity, the conduction can be assumed isotropic. Also, in this case the Ampère force $(1/4\pi)\,\mathrm{curl}\,\mathbf{B}\times\mathbf{B}$ is much smaller than that resulting from the pressure gradient and therefore can be neglected. Disregarding other forces, such as resulting from gravity, rotation, etc., we arrive at the basic model problem of a three-dimensional

nonlinear dynamics of an optically thin isotropic plasma, which is subject to external heating and cools radiatively. As we shall see, this model, though greatly simplified, is quite nontrivial.

If the characteristic spatial dimensions of the plasma region of interest are much less than the acoustic Field length (the characteristic distance traveled by acoustic waves on the radiation time scale), while the time scales we are interested in are much longer than the acoustic time, the pressure gradients become small. If, in addition, the plasma dimensions are much larger than the conductive Field length (the characteristic thermal diffusion distance on the radiation time scale), one can neglect the heat conduction (at least, in the initial stage of the dynamics). This regime was first considered by Sasorov [8] in the three-dimensional geometry. Sasorov employed the isobaricity condition p =const, which assumes that the plasma region of interest is surrounded by an external (inexhaustible) plasma "reservoir" providing a free mass exchange between the internal and external plasma. Assuming a heating-cooling function with only one, unstable equilibrium, Sasorov showed that the formation of "thermal pancakes," earlier predicted in the long-wavelength limit of the RCI [7], persists in the intermediate-wavelength limit as well. The isobaric regime of the intermediate-wavelength RCI was also studied in a one-dimensional geometry [9–11], but for a bistable heating-cooling function. In this case, the plasma segregates into two locally stable phases. Then heat conduction becomes important, and the final stage of the dynamics is described in terms of "evaporation" or "condensation" fronts [18,19,10], which normally lead to "uniformization" of the plasma.

In the present work we shall also consider a bistable plasma. However, as in our previous paper [12] (which will be called AMS in the following), we shall be interested in a regime alternative to isobaricity and assume that the plasma is confined by external forces, so that no plasma can enter or leave the system. As an astrophysical example of such a confinement, one can consider interstellar gas in the gravitational field of a galactic disk. Of course, a fully consistent treatment of such a problem would require an explicit account of gravitation in the equation of motion. Instead, we effectively replace a smooth potential well of the gravity field by a "box," so that the plasma inside the "box" does not feel the gravity until it reaches the "walls."

AMS treated the nonlinear dynamics of the RCI of a confined, thermally bistable plasma in the planar geometry. As the length of the system is much larger than the conductive Field length, the width of the "evaporation" or "condensation" fronts is very small compared to the length of the system. It was shown by AMS that nonlocality, resulting from the mass conservation and the finite length of the system, makes possible formation of stable stationary coherent patterns in the form of two phases, divided by narrow transition layers (fronts). Correspondingly, during the conductive stage, the spatially uniform, time-dependent plasma pressure $P(t)$ approaches the "area rule" value P_* (see below), so that the "evaporation" or "condensation" front motions are arrested. From the viewpoint of pattern formation theory, the one-dimensional system considered by AMS exemplifies a bistable system, subject to a nonlocal constraint (total mass conservation). Other examples of nonlocally constrained systems can be found in entirely different fields of physics and chemistry [20–23].

In the two- and three-dimensional cases, the conductive stage of the RCI becomes more complex, as two new factors, front curvature and deformation instability of the traveling fronts, can affect the dynamics. The front curvature of large-scale patterns is small and therefore might seem insignificant. However, we shall see that, as the pressure approaches P_* and the front motion slows down, the curvature effects become dominant and determine both the possible final states of the system and the dynamics of relaxation towards the final states. The major aim of this paper is to investigate in some detail, analytically and numerically, the role of the curvature effects in the dynamics of confined bistable plasmas. Deformation instability of "evaporation" fronts and its possible consequences in the dynamics of the system are briefly considered in Appendix A.

The present paper is organized in the following way. In Sec. II we formulate the problem, introduce the necessary notation, and deal with the intermediate- and short-wavelength limits. An essential moment here is elimination of the acoustic mode from the reduced equations. In Sec. III large-scale two-phase equilibria, specific for thermally bistable plasmas, are considered. We start with a model problem of the equilibrium of a large spherical "drop" (or "bubble") of one phase in the other phase and arrive at a linear relationship between the curvature of the drop surface and the corresponding correction to the area-rule value of the pressure. This relation is then generalized to nonspherical drops and bubbles and employed for delineating possible large-scale equilibrium patterns in the system. The next step is a further reduction of the governing equations, in order to describe the dynamics of a radiatively segregated plasma (Sec. IV). The obtained "super-reduced" equations are employed in Secs. V and VI. Section V concerns stability analysis of the large-scale equilibria. A number of model problems is solved analytically. Stability of parallel slabs and individual drops (bubbles) is studied, and the minimum possible radius of a stable drop (bubble) is found. In Sec. VI the dynamics of ensembles of drops (bubbles) interacting and competing via evolving background is considered. This competition looks like Ostwald ripening, and we address the dynamical and statistical properties of this system. In Sec. VII we perform two-dimensional numerical simulations of the dynamics of a bistable plasma, confined in a square "box." Sec. VIII is devoted to a brief summary and discussion of the results.

II. BASIC EQUATIONS AND THE ACOUSTIC MODE ELIMINATION

We start with simple fluid equations, describing the dynamics of an unmagnetized, optically thin ideal plasma of mass density ρ, temperature T, and velocity $\mathbf{v}$, which

is heated externally and cools radiatively [2]:

$$\frac{d\rho}{dt} + \rho\nabla\cdot\mathbf{v} = 0, \tag{1}$$

$$\rho\frac{d\mathbf{v}}{dt} + \nabla p = \mathbf{0}, \tag{2}$$

$$\frac{1}{\gamma-1}\frac{dp}{dt} + \frac{\gamma}{\gamma-1}p\nabla\cdot\mathbf{v} + \rho\mathcal{L}(\rho,T) - \nabla\cdot(K\nabla T) = 0, \tag{3}$$

$$p = \frac{R}{\mu}\rho T, \tag{4}$$

where $d/dt = \partial/\partial t + \mathbf{v}\cdot\nabla$ is the total time derivative, $\mathcal{L}$ is the heating-cooling function (the difference between the rate of radiative cooling and the rate of heating per unit mass), $K = K(T)$ is the (isotropic) thermal conductivity, γ is the specific heat ratio, μ is the effective molar mass of the plasma, and R is the gas constant. All forces except the pressure gradient are disregarded in the equation of motion (2). As to the small viscosity, it can be neglected for slow (subacoustic) motions that we shall be interested in.

The linear stability of the simplest, uniform equilibria of the system (1)–(4), i.e. $\rho = \rho_0$ =const, $T = T_0$==const, $\mathbf{v} = \mathbf{0}$, and $\mathcal{L}(\rho_0, T_0) = 0$, was studied by Field [2]. It is the behavior of the heating-cooling function $\mathcal{L}(\rho, T)$ in the vicinity of the equilibrium values ρ_0 and T_0, the perturbation wave number $k = (k_x^2 + k_y^2 + k_z^2)^{1/2}$, and the value of thermal conductivity K which control thermal stability and, in the case of instability, its type (isochoric, isobaric, or isentropic) and growth rate [2]. In the intermediate- and short-wavelength limits, the results of the linear theory of the RCI look as follows. If the uniform plasma equilibrium is *isochorically* stable,

$$\left(\frac{\partial\mathcal{L}}{\partial T}\right)_\rho > 0 \tag{5}$$

(and only this case will be considered in the following), it is the *isobaric* instability criterion,

$$\left(\frac{\partial\mathcal{L}}{\partial T}\right)_p = \left(\frac{\partial\mathcal{L}}{\partial T}\right)_\rho - \frac{\rho}{T}\left(\frac{\partial\mathcal{L}}{\partial\rho}\right)_T < 0 \tag{6}$$

for $\rho = \rho_0$ and $T = T_0$ which represents the necessary condition for the RCI [2]. The instability is aperiodic, and its growth rate is [2]

$$n = \frac{(\gamma-1)\mu}{\gamma R}\left[-\left(\frac{\partial\mathcal{L}}{\partial T} - \frac{\rho_0}{T_0}\frac{\partial\mathcal{L}}{\partial\rho}\right) - \kappa_0 k^2\right], \tag{7}$$

evaluated at $T = T_0$ and $\rho = \rho_0$. Here $\kappa_0 = K(T_0)/\rho_0$ is the unperturbed thermal diffusivity. As seen from Eq. (7), thermal conduction always has a stabilizing effect, erasing perturbations with wavelengths shorter than some threshold one (which typically is of the order of the Field conductive length).

We shall consider a plasma confined in some domain Ω (two or three dimensional), the maximal dimension of which is L. We assume that the normal components of the plasma velocity and of the heat flux at the closed boundary Γ of the domain Ω are zero:

$$(\mathbf{v}\cdot\mathbf{n}_\Omega)|_\Gamma = 0, \tag{8}$$

$$(\nabla T\cdot\mathbf{n}_\Omega)|_\Gamma = 0, \tag{9}$$

where $\mathbf{n}_\Omega$ is the normal to the boundary Ω. From Eqs. (1) and (8) immediately follows mass conservation:

$$\int_\Omega \rho(\mathbf{r},t)d\mathbf{r} = \text{const}. \tag{10}$$

If the dimensions of the system are much less than the acoustic Field length, while the plasma motions are slow in comparison with the speed of sound c_s, we can simplify the original set of Eqs. (1)–(4), so that the reduced system will not include the acoustic modes [24]. For this purpose, let us represent the total plasma pressure $p(\mathbf{r},t)$ as a sum of its spatially averaged part

$$P(t) = \frac{1}{|\Omega|}\int_\Omega p(\mathbf{r},t)\,d\mathbf{r} \tag{11}$$

and a spatially variable part $\tilde{p}(\mathbf{r},t)$, so that

$$p(\mathbf{r},t) = P(t) + \tilde{p}(\mathbf{r},t), \tag{12}$$

where $|\Omega|$ is the volume of the region Ω in the three-dimensional case or its area in the two-dimensional case. As the ratio $\tilde{p}/P \sim v^2/c_s^2$ is assumed to be small, we can neglect $\tilde{p}$ in Eqs. (3) and (4). Therefore, the set of Eqs. (1)–(4) can be rewritten as

$$\frac{d\rho}{dt} + \rho\nabla\cdot\mathbf{v} = 0, \tag{13}$$

$$\rho\frac{d\mathbf{v}}{dt} + \nabla\tilde{p} = \mathbf{0}, \tag{14}$$

$$\frac{1}{\gamma-1}\frac{dP}{dt} + \frac{\gamma}{\gamma-1}P\nabla\cdot\mathbf{v} + \rho\mathcal{L}(\rho,T) - \nabla\cdot(K\nabla T) = 0, \tag{15}$$

$$P(t) = \frac{R}{\mu}\rho T, \tag{16}$$

with the boundary conditions (8) and (9). In view of Eq. (16) we can also write

$$(\nabla\rho\cdot\mathbf{n}_\Omega)|_\Gamma = 0. \tag{17}$$

Note that $\tilde{p}$ appears only in Eq. (14), and it can be eliminated completely if we apply curl to both sides of this equation. The resulting relation

$$\nabla\times\left(\rho\frac{d\mathbf{v}}{dt}\right) = \mathbf{0} \tag{18}$$

replaces Eq. (14). In this sense, Eqs. (13)–(16) with the boundary conditions (8) and (9) represent a closed set. These equations serve as the general form of our reduced model, applicable to the intermediate- and short-wavelength limits. It can be checked that linear stability analysis of uniform equilibria in the framework of the reduced set of equations (13)–(16) immediately yields expression (7) for the growth rate.

Integrating Eq. (15) over the volume of the region Ω and using the boundary conditions, we obtain the following important relation:

$$\dot{P}(t) = -\frac{\gamma - 1}{|\Omega|} \int_{\Omega} \rho \mathcal{L}(\rho, T) d\mathbf{r}, \tag{19}$$

which determines the temporal evolution of the average plasma pressure. Equation (19) describes the global energy balance of the system and is similar to the "global pressure equation" of Begelman and McKee [25]. Its one-dimensional version was employed in AMS.

Now we shall follow AMS and assume that the temperature dependence of the heat conductivity is power-like, $K(T) = K_0 T^{\alpha}$, so that the cases of electron-dominated ($\alpha = 5/2$) and neutral-dominated ($\alpha = 1/2$) thermal conductivity can be accounted for properly. Instead of the plasma density, we introduce the specific volume $u(\mathbf{r}, t) = \rho^{-1}(\mathbf{r}, t)$ and eliminate the temperature, using the equation of state (16). Now the heating-cooling function $\mathcal{L}(\rho, T) = \mathcal{L}[u^{-1}, (\mu/R)Pu]$ depends on u and P. Introducing scaled variables $\hat{u} = u/u_0$ and $\hat{P} = P/P_0$, we define the dimensionless heating-cooling function $\lambda(\hat{u}, \hat{P})$:

$$\frac{\gamma - 1}{\gamma p u} \mathcal{L}\left(u^{-1}, \frac{\mu}{R} P u\right) = \mathcal{L}_0 \lambda(\hat{u}, \hat{P}), \tag{20}$$

where the parameters u_0 and P_0 and the coefficient $\mathcal{L}_0$ are chosen in such a way that the function $\lambda(\hat{u}, \hat{P})$ evaluated, for example, at $\hat{u} = 1$ and $\hat{P} = 1$ is equal to unity. Following Begelman and McKee [25], we define the conductive Field length δ_F. In our notation,

$$\delta_F^2 = \left(\frac{\mu}{R}\right)^{1+\alpha} \frac{(\gamma - 1) K_0 P_0^{\alpha} u_0^{1+\alpha}}{\gamma \mathcal{L}_0}. \tag{21}$$

Recall that intermediate wavelengths are much longer than δ_F (however, much shorter than the acoustic Field length, see above), while short wavelengths are comparable to or smaller than δ_F.

Now we can introduce the remaining scaled variables: $\hat{\mathbf{r}} = \mathbf{r}/\delta_F$, $\hat{t} = \mathcal{L}_0 t$, and $\hat{\mathbf{v}} = \mathbf{v}/(\delta_F \mathcal{L}_0)$, and rewrite Eqs. (13)–(15) in the following scaled form:

$$\frac{du}{dt} = u \nabla \cdot \mathbf{v}, \tag{22}$$

$$\frac{d\mathbf{v}}{dt} + u \nabla \tilde{p} = \mathbf{0}, \tag{23}$$

$$\frac{\dot{P}}{\gamma P} + \nabla \cdot \mathbf{v} + \lambda(u, P) - P^{\alpha} \nabla \cdot (u^{\alpha} \nabla u) = 0 \tag{24}$$

with the boundary conditions (8) and

$$(\nabla u \cdot \mathbf{n}_{\Omega})|_{\Gamma} = 0 \ . \tag{25}$$

The global pressure equation (19) can be rewritten as

$$\frac{\dot{P}}{\gamma P} = -\frac{1}{|\Omega|} \int_{\Omega} \lambda(u, P) \, d\mathbf{r}, \tag{26}$$

and the carets are omitted.

III. LARGE-SCALE SEGREGATED EQUILIBRIA

Let us look for possible *segregated*, that is *nonuniform* equilibria, $v = \partial/\partial t = 0$, of Eqs. (22)–(24), satisfying the boundary condition (25). These are described by the following equation:

$$\nabla \cdot (u^{\alpha} \nabla u) = P_{eq}^{-\alpha} \lambda(u, P_{eq}), \tag{27}$$

where P_{eq} is the equilibrium pressure.

Notice that if they exist the equilibria described by Eq. (27) coincide with those of the original (unreduced) set of equations (1)–(4). Also, Eq. (27) will hold in the *isobaric* regime, the difference being in the selection of the parameter P_{eq}: in the isobaric regime P_{eq} is prescribed by the boundary conditions. Equations similar to Eq. (27) appear in many contexts. For example, the same equation describes possible equilibria of a one-component reaction-diffusion equation [26]:

$$\frac{\partial u}{\partial t} = -P^{-\alpha} \lambda(u, P) + \nabla \cdot (u^{\alpha} \nabla u). \tag{28}$$

Finally, in the two-dimensional case, Eq. (27) with $\alpha = 0$ describes a steady vortex flow of an ideal incompressible fluid [27]. In this case u plays the role of a stream function, so that the vorticity is equal to $\nabla^2 u$. Obviously, *stability* of the solutions to Eq. (27) in all the above-mentioned problems depends on the specific *time-dependent* governing equations and looks differently in all these problems.

Although the one-dimensional problem for Eq. (27) is elementary, not much is known about two- and three-dimensional analytic solutions, unless the function $\lambda(u, P)$ is a linear function of $u^{\alpha+1}$. A limited number of particular exact solutions can be found in the literature for specially selected nonlinear $\lambda(u, P)$. Instead, we shall consider here more general, though approximate, *large-scale* solutions, which describe segregation of a *bistable* plasma into large regions occupied by the stable phases 1 (where $u = u_1$) and 2 (where $u = u_2$), with narrow transition layers between them. Therefore we shall concentrate, as in the paper AMS, on the bistable heating-cooling function $\lambda(u, P)$. For a fixed P, such a function has an "unstable" root $u_u(P)$, surrounded by two "stable" roots, so that $u_1(P) < u_u(P) < u_2(P)$. For large-scale segregated equilibria, both the right and the left hand side of Eq. (27) are close to zero everywhere except in these transition layers. Therefore Eq. (27) is satisfied "trivially" outside the transition layers, while the "non-trivial" balance between the left and right hand sides of Eq. (27) determines the structure of the transition layers.

The simplest large-scale segregated equilibria are those with *zero* curvature, and they represent alternating parallel plasma slabs with $u = u_1(P_{eq})$ and $u = u_2(P_{eq})$

whose widths are much larger than unity. In this case Eq. (27) becomes one dimensional, and we recover the well known solution discussed by AMS. In this case, the equilibrium pressure P_{eq} is equal (with an exponentially high accuracy) to a special value P_*, corresponding to the area rule.

The simplest solutions with a *nonzero* curvature represent a single cylindrical or spherical "drop" (phase 1) in the "vapor" (phase 2), or, alternatively, "bubble" (phase 2) in the "liquid" (phase 1). In these cases, Eq. (27) can be rewritten as

$$\frac{d}{dr}\left(u^\alpha \frac{du}{dr}\right) + \frac{d-1}{r} u^\alpha \frac{du}{dr} = P_{eq}^{-\alpha}\lambda(u, P_{eq}), \qquad (29)$$

where $d = 2$ for a circle (in two dimensions) or cylinder (in three dimensions), and 3 for a sphere. (This and most of the following relations containing d are formally valid in the planar case $d = 1$ as well.) Equation (29) with the boundary condition (25) represents a nonlinear eigenvalue problem for the eigenfunction $u(r)$ and eigenvalue P_{eq}. We consider in this paper only large-scale drops and bubbles, the radius of which, R, is much larger than unity. In this case, the eigenvalue problem can be treated perturbatively. As the zero approximation, we shall consider the corresponding planar problem in an infinite space (see, e.g., AMS). In this approximation $P_{eq} = P_*$, the area-rule value. Being interested in finding a small (linear) correction to P_{eq}, proportional to $1/R$, we can make the following simplifications. First, we can move the boundary condition at $r = 0$ to $-\infty$ (which gives only an *exponentially* small error in P_{eq}). Second, we can replace the factor $1/r$ by $1/R$ in the second term of Eq. (29), because at $|r - R| \gg 1$ $\partial u/\partial r$ is exponentially small, while at $|r - R| \sim 1$ the factor $1/r$ can be written as

$$\frac{1}{r} = \frac{1}{R} - \frac{r-R}{R^2} + \cdots ;$$

therefore it can be replaced by $1/R$ with an error $O(R^{-2})$, which we neglect in the linear approximation. [The procedure of replacement of $1/r$ by $1/R$ in the second term of Eq. (29) is well known in the theory of two-dimensional reaction-diffusion equations; see, e.g., [28].] Therefore, at $R \gg 1$, the second term in Eq. (29) is much smaller than the first one. In the zero approximation, we neglect the second term and return to the one-dimensional equilibrium problem. This yields the area-rule [18,19]

$$\int_{u_1(P)}^{u_2(P)} u^\alpha \, \lambda(u, P)\, du = 0, \qquad (30)$$

so that $P_{eq} = P_*$, the area-rule value. Correspondingly, for the zero-order approximation of the function u we have the following relation (see AMS):

$$\frac{1}{2}\left(\frac{du_0}{dr}\right)^2 u_0^{2\alpha} = P_*^{-\alpha} \int_{u_1(P_*)}^{u_0} u^\alpha \lambda(u, P_*) du. \qquad (31)$$

In the *first* approximation, we can expand $\lambda(u, P)$ in the vicinity of $P = P_*$:

$$\lambda(u, P) \approx \lambda(u, P_*) + \mu(u)(P - P_*), \qquad (32)$$

where $\mu(u) = \partial\lambda(u, P)/\partial P$ evaluated at $P = P_*$, and $P - P_* \ll P_*$.

Now we multiply Eq. (29) by $u^\alpha du/dr$ and integrate it over r from 0 to the boundary Γ of the plasma region. Then we make use of the fact that du/dr vanishes outside the transition layer, replace (under the integral) the function u and its derivative du/dr by their zero-order approximations in the first-order terms, and employ Eqs. (30) and (31). We arrive at the following relation:

$$P_{eq} = P_* + \frac{f}{g}\mathcal{K}, \qquad (33)$$

where

$$f = P_*{}^\alpha \quad \frac{\int_{u_1}^{u_2} u^\alpha \left(\int_{u_1}^{u} \eta^\alpha \lambda(\eta, P_*) d\eta\right)^{1/2} du}{\int_{u_1}^{u_2} \left(\int_{u_1}^{u} \eta^\alpha \lambda(\eta, P_*) d\eta\right)^{1/2} du}, \qquad (34)$$

$$g = \frac{P_*{}^{\alpha/2} \int_{u_1}^{u_2} u^\alpha \, \mu(u)\, du}{\int_{u_1}^{u_2} \left(2\int_{u_1}^{u} \eta^\alpha \, \lambda(\eta, P_*)\, d\eta\right)^{1/2} du}. \qquad (35)$$

Therefore we have obtained a linear relationship between the small correction $P_{eq} - P_*$ to the area-rule value P_* and the small (dimensionless) curvature $\mathcal{K}$ of an equilibrium drop. The curvature $\mathcal{K} = \pm(d-1)/R$ is defined here to be positive for a drop and negative for a bubble. The g factor (35) appeared in the one-dimensional theory (see AMS), while the f factor is new. Notice that f is always positive, which is important for the following analysis. For the simplest case of $\alpha = 0$ (temperature-independent conductivity), $f = 1$.

Equation (33) has been derived for "perfectly" cylindrical or spherical drops and bubbles. However, its validity can be extended. First, if we neglect the transition layer width, we can use the term "surface" for our drops and bubbles. Let us consider a large and, in general, *non*-spherical drop (bubble), the surface of which is smooth. It is important that the nonsphericity does not have to be small, so that any *large-scale* object with a *smooth* surface can be considered. By smoothness we mean the curvature to be much smaller than the inverse conductive Field length (that is, than unity in the scaled equations), while the typical length of the curvature variations along the surface is much larger than the conductive Field length (again unity). We prove in Appendix B that, starting from Eq. (27) and introducing local orthogonal coordinates on the surface of the nonspherical drop or bubble, we arrive again at Eq. (33), but now

$$\mathcal{K} = \nabla \cdot \mathbf{n}|_{s=0}\,, \qquad (36)$$

where $\mathbf{n}$ is a smooth unit vector field, which is normal to the surface of the drop (bubble), and directed from the phase 1 to the phase 2, while the point $s = 0$ is the base of the vector $\mathbf{n}$ on the surface of the drop. This result is obtained in the limit of a large drop (bubble)

radius R (see Appendix B for a more precise condition), and it is valid with an accuracy of R^{-2}. Equation (36) implies that the quantity $\mathcal{K}$ represents the sum of the two principal curvatures of the interface [29]:

$$\mathcal{K} = 1/R_1 + 1/R_2. \tag{37}$$

In its new meaning, Eq. (33) has far reaching consequences. Since the equilibrium pressure must be uniform, any equilibrium object must satisfy (with an accuracy of R^{-2}) the condition of a *constant sum of the principal curvatures* of its surface [30]. Therefore a drop or bubble of an *arbitrary* form is generally *not* in equilibrium. Furthermore, if there is an *ensemble* of large drops (or bubbles), whose distances from each other and from the boundary Ω are much larger than unity, then an equilibrium can be achieved only if the radii of *all* the drops (bubbles) are equal.

Most natural are "detached" equilibria, not connected to the boundary Γ. It is a well known fact of differential geometry that the only detached objects with a constant sum of the principal curvatures of their surfaces are *perfect* spheres. (This is the reason why a weightless soap bubble, not connected to any boundary, always acquires a perfectly spherical shape.) Therefore, in view of Eq. (33), we see that the equilibrium drops or bubbles must either be perfectly spherical or perfectly cylindrical, and they must have *the same radius.* (Formally, cylindrical drops and bubbles belong to the "attached" equilibria.) In two dimensions, we have only perfectly circular "drops" and "bubbles" as equilibrium objects.

It is interesting to consider also some "attached" equilibria. The simplest of them are the above-mentioned alternating parallel strips (in two dimensions) and slabs (in three dimensions) of segregated plasma. As we shall see, these can arise naturally in rectangular "boxes," like one that we shall use in our numerical simulations (Sec. VII). Also, spherical drops (bubbles) of the same radius, coexisting with cylindrical drops (bubbles) of *half* of this radius can be in equilibrium.

In general, quite complex attached equilibrium patterns, satisfying both the equation

$$1/R_1 + 1/R_2 = \mathcal{K} = \text{const} \tag{38}$$

with variable R_1 and R_2 and the prescribed boundary conditions, are possible. Although interesting and mathematically nontrivial, such patterns are nongeneric. In particular, their existence can be quite sensitive to the specific form of the boundary Γ [31].

In summary, we have identified possible large-scale equilibrium patterns. We shall see, however, that stability arguments introduce important additional limitations.

IV. CONDUCTIVE RELAXATION: "SUPER-REDUCED" EQUATIONS AND THEIR LINEARIZATION

In the relatively fast, radiative stage of the RCI, the confined bistable plasma segregates into two locally stable phases. The following slower dynamics is determined by thermal conduction, and we call this stage conductive relaxation. Our immediate aim is to obtain "super-reduced" equations, which will enable us, in particular, to follow the relaxation of the system to any of the equilibria found in the previous section.

At the end of the radiative stage, the plasma density and temperature of each of the two phases become close to uniform outside the narrow transition layers, so that we describe these phases by the uniform values of their specific volume $u_1(P)$ and $u_2(P)$ (therefore neglecting $\tilde{p}$ compared to P everywhere except in ∇p). Following $P(t)$, u_1 and u_2 can vary in time. Therefore, for the phase i ($i = 1, 2$), the continuity equation (22) can be rewritten as

$$\nabla \cdot \mathbf{v}_i = \frac{\partial \ln u_i(P)}{\partial P} \dot{P}, \tag{39}$$

while Eq. (23) takes the following form:

$$\frac{d\mathbf{v_i}}{dt} + u_i(P) \nabla \tilde{p}_i = \mathbf{0}. \tag{40}$$

Taking the curl of Eq. (40), we obtain

$$\frac{\partial}{\partial t} \nabla \times \mathbf{v}_i = \nabla \times [\mathbf{v}_i \times (\nabla \times \mathbf{v}_i)]. \tag{41}$$

Equations (39)–(41) should be supplemented by matching conditions at each interface dividing the regions occupied by the phases 1 and 2. In doing so, we treat the narrow transition layers as discontinuities. This implies, in particular, that the velocity field is assumed to be large scale, so that it has no components with wavelengths comparable to the conductive Field length.

As usual, the continuity and momentum equations result in the following matching conditions (see, e.g., [32]):

$$v_{i\,n} = c_n + j_n u_i \qquad (i = 1, 2), \tag{42}$$

$$\frac{v_{1\,n} - c_n}{u_1} \mathbf{v}_{1\,t} = \frac{v_{2\,n} - c_n}{u_2} \mathbf{v}_{2\,t}, \tag{43}$$

$$u_1 \left(\frac{v_{1\,n} - c_n}{u_1} \right)^2 + \tilde{p}_1 = u_2 \left(\frac{v_{1\,n} - c_n}{u_1} \right)^2 + \tilde{p}_2. \tag{44}$$

Here $w_n = \mathbf{w} \cdot \mathbf{n}$ is the normal component of any vector $\mathbf{w}$ at each interface, and $\mathbf{w_t} = \mathbf{w} - (\mathbf{w} \cdot \mathbf{n})\mathbf{n}$. The normal vector $\mathbf{n}$ was defined in Sec. 3, c_n is the normal component of the front velocity, and $j_n = (v_{in} - c_n)/u_i$ is the flux of material through the interface.

In its turn, the thermal balance equation provides an expression for j_n. To get it, one should transfer to the reference frame, which moves with the velocity c_n, use the smallness of the transition layer width, and match the "inner" and "outer" solutions, as in the one-dimensional theory of AMS. Obviously, j_n depends on the pressure P and front curvature $\mathcal{K}$. For small $\mathcal{K}$, this dependence can be written in the following form:

$$j_n = -G(P) + F(P)\mathcal{K}, \tag{45}$$

where $G(P)$ and $F(P)$ are unknown functions. It is difficult to calculate these functions in the general case, as it requires solving a nonlinear eigenvalue problem for an ordinary differential equation of the second order (which follows from the thermal balance equation in the reference frame, moving with the interface). However, they can be easily found in the limit of $|P - P_*| \ll P_*$, when the pressure P is already close to its area-rule value. Expanding $G(P)$ and $F(P)$ in a Taylor series near $P = P_*$, we have

$$G(P) = G(P_*) + G'(P_*)(P - P_*) + \cdots, \tag{46}$$

$$F(P) = F(P_*) + \cdots, \tag{47}$$

and the terms denoted by $\cdots$ can be neglected as soon as $|P - P_*| \ll P_*$. Owing to the definition of P_* we have $G(P_*) = 0$, so that

$$j_n = -G'(P_*)(P - P_*) + F(P_*)\mathcal{K}. \tag{48}$$

Comparing Eq. (48) with Eq. (33) and with Eq. (32) of AMS, we see that $G'(P_*) = g$ and $F(P_*) = f$. Finally,

$$j_n = -g(P - P_*) + f\mathcal{K} \quad \text{for} \quad |P - P_*| \ll P_*. \tag{49}$$

It is seen that both the one-dimensional result of AMS,

$$j_n = -g(P - P_*), \tag{50}$$

and the equilibrium relation (33) are recovered from Eq. (49) as limiting cases.

Equations (8) and (25) remain the boundary conditions for the system. In the segregated plasma that we are considering now, Eq. (25) is satisfied automatically at the parts of the boundary Γ embracing regions occupied by either of the "pure" phases 1 and 2. Also, if an interface meets the boundary Γ, the boundary conditions require each interface to be perpendicular to the boundary at their "meeting point."

Equations (39) and (40), combined with the matching conditions (42) – (44) and (49) at the interfaces and the boundary conditions, represent a closed set and describe the dynamics of confined thermally bistable plasmas at the conducting stage, when $|P - P_*| \ll P_*$. However, it is very helpful to find the corresponding "super-reduced" forms for the global pressure equation (26) and mass conservation law (10) in the limit of small $(P - P_*)/P_*$ and $\mathcal{K}$. Integrating each of the two Eqs. (39) over all domains occupied by the phases 1 and 2, respectively, and using the Gauss theorem, Eqs. (42), and the boundary condition (8), we get

$$\left(|\Omega_1|\frac{\partial \ln u_1(P)}{\partial P_*} + |\Omega_2|\frac{\partial \ln u_2(P)}{\partial P_*}\right)\dot{P}$$

$$= \int\int_{\Omega_I} (v_{1\,n} - v_{2\,n})\, dS$$

$$= [u_1(P_*) - u_2(P_*)] \int\int_{\Omega_I} j_n\, dS, \tag{51}$$

where a surface integral over all interfaces Ω_I appears. Then, using Eq. (49), we arrive after some algebra at the following equation:

$$\dot{P} = \frac{P - P_* - \langle\mathcal{K}\rangle f/g}{\langle L\rangle} \times \left(\frac{g(u_2 - u_1)^2\langle u\rangle}{(u_2 - \langle u\rangle)\frac{\partial u_1}{\partial P} + (\langle u\rangle - u_1)\frac{\partial u_2}{\partial P}}\right)_{P=P_*}. \tag{52}$$

This reduced form of the global pressure balance equation (26) generalizes the corresponding one-dimensional result [Eq. (37) of AMS]. The following notation has been used in Eq. (52):

$$S = \int\int_{\Omega_I} dS \tag{53}$$

is the total area of the interfaces,

$$\langle L\rangle = \frac{|\Omega|}{S} \tag{54}$$

is the characteristic size of segregated objects, and

$$\langle\mathcal{K}\rangle = \frac{1}{S}\int\int_{\Omega_I} \mathcal{K}\, dS \tag{55}$$

is the sum of the two principal curvatures, averaged over the interfaces. Finally,

$$\langle u\rangle = \frac{|\Omega|}{|\Omega_1|/u_1(P) + |\Omega_2|/u_2(P)} = |\Omega|\left(\int_\Omega \frac{d\mathbf{r}}{u(\mathbf{r},0)}\right)^{-1} \tag{56}$$

is the average specific volume. This quantity is defined by the first equality of Eq. (56). The second equality shows that $\langle u\rangle$ is independent of time, which implies that mass conservation holds in the reduced equations. This fact can be checked directly, if we differentiate the expression $|\Omega_1|/u_1(P) + |\Omega_2|/u_2(P)$ with respect to time, using the relations

$$\frac{d}{dt}|\Omega_1| = -\frac{d}{dt}|\Omega_2| = \int\int_{\Omega_I} c_n\, dS, \tag{57}$$

Eqs. (39), and the Gauss theorem.

Returning to the global pressure equation (52), we immediately see an important difference between the one-dimensional case ($\mathcal{K} = 0$) and the higher-dimensional cases. The expression in the large parentheses of Eq. (52) is negative (see AMS). Therefore, on the time scale $\tau_1 \sim \langle L\rangle$, the pressure mismatch $P - P_*$ approaches $f\langle\mathcal{K}\rangle/g$ (which was zero in the one-dimensional theory). At the next (slower) stage, $P - P_*$ is approximately equal to $f\langle\mathcal{K}\rangle/g$. As the average curvature $\langle\mathcal{K}\rangle$ is (slowly) time dependent, $P - P_*$ follows $f\langle\mathcal{K}\rangle/g$ "adiabatically." The time dependent quantity $\langle\mathcal{K}\rangle$, which does not appear in the one-dimensional problem, introduces a new "degree of freedom," and, therefore, a new time scale τ_2; see later. We shall see in the next two sections that this can result in qualitatively new effects, such as instability with respect to small changes in the sizes of "drops" and "bubbles," Ostwald ripening, etc.

Now we present the linearized version of the super-reduced equations, which will be employed in the next section for the analysis of the *linear* stability of the equilibria found in Sec. III. The linearization is performed near a static equilibrium, so that the unperturbed velocity is put to zero. The linearized continuity equation still looks like Eq. (39), except that the P derivative in the right hand side should be evaluated now at $P = P_*$. The linearized Euler equation (40) takes the form

$$\frac{\partial \mathbf{v_i}}{\partial t} + u_i(P_*)\nabla \tilde{p}_i = \mathbf{0}, \tag{58}$$

while Eq. (41) yields

$$\frac{\partial}{\partial t}(\nabla \times \mathbf{v}_i) = \mathbf{0}. \tag{59}$$

This means that, if the flow outside the transition layers is potential at $t = 0$, it remains potential for all times. Furthermore, if the initial velocity is zero, we can introduce, instead of the pressure variation $\tilde{p}_i$, the following effective potential

$$\psi_i(\mathbf{r}, t) = -\int_0^t \tilde{p}_i(\mathbf{r}, t')dt', \tag{60}$$

and replace Eq. (58) by the following relation:

$$\mathbf{v_i} = u_i(P_*)\nabla\psi_i. \tag{61}$$

Linearization of the matching conditions (42)–(44) give the following results. In Eq. (42) we evaluate u_i at $P = P_*$:

$$v_{i\,n} = c_n + j_n u_i(P_*)\ . \tag{62}$$

In the linear approximation, Eq. (43) is satisfied identically. In Eq. (44) the terms proportional to the square of the velocities can be neglected, so that it can be finally written as a continuity condition:

$$\psi_1 = \psi_2. \tag{63}$$

V. PERFECT PATTERNS AND BACKGROUND-MEDIATED INSTABILITY

In this section we shall study analytically a number of two- and three-dimensional stability problems for the equilibria found in Sec. III. These problems are described by the linearized super-reduced equations derived in Sec. IV. We shall start in Sec. V A with stability of a planar equilibrium interface with respect to small volumetric ($k = 0$) and deformation ($k \neq 0$) perturbations. Stability of a perfect drop (bubble) with respect to deformation of its shape is analyzed in Sec. V B. Radial stability of the same drop (bubble) is considered in Sec. V C.

A. Linear stability of a planar interface

Let the two-dimensional confinement domain Ω represent a rectangle with the dimensions L_x and L_y, and let the unperturbed interface between phases 1 and 2 be parallel to the x axis and positioned at $y = \Delta_1$ (see Fig. 1). As usual, indices 1 and 2 correspond to the phases 1 and 2, respectively. Now, let $\delta(x, t)$ be a small perturbation of the interface position. We expand it in the Fourier series $\delta(x, t) = \sum_k \delta_k(t) \cos kx$. As close to equilibrium the interface is normal to the boundary at the intersection points, the wave numbers k must be equal to $\pi n/L_x$, where $n = 0, 1, 2, \ldots$. The perturbation includes both the interface deformations, $n > 0$, and the "volumetric" mode $n = 0$. In general, the perturbed interface is not in equilibrium, therefore the system will start to evolve. Will the interface return to its equilibrium form (possibly after a small displacement), and, if yes, how much time will it take? The answer to this question is determined by the behavior of the functions $\delta_k(t)$, and we should find them. We start with the linearized Eqs. (39) for the velocity fields in the regions of the perturbed phases 1 and 2. Using the relation (61), we rewrite Eqs. (39) as two Poisson equations for $\psi_{1,2}$:

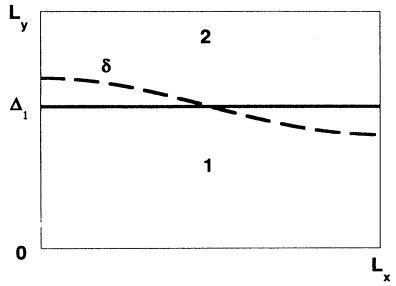

FIG. 1. Geometry of the problem of linear stability of a slab-type equilibrium. Shown are the unperturbed (solid line) and perturbed (dashed line) interfaces between the phases 1 and 2.

$$\nabla^2\psi_{1,2} = C_{1,2}(t), \tag{64}$$

where

$$C_{1,2}(t) = \frac{1}{u_{1,2}(P_*)}\frac{\partial \ln u_{1,2}}{\partial P_*}\dot{P}, \tag{65}$$

and $\partial u_{1,2}/\partial P_*$ stands for $\partial u_{1,2}/\partial P$ evaluated at $P = P_*$. The solutions to Eq. (64) can be sought in each of the two domains 1 and 2 as the sum of its particular solution and a harmonic function, both of them satisfying the condition (8) on the boundary Γ. With Eq. (61) for the velocity, the boundary condition (8) is reduced to the requirements that the x derivatives of the potentials $\psi_{1,2}$ vanish at $x = 0$ and $x = L_x$, while their y derivatives vanish at $y = 0$ and $y = L_y$. The following expressions meet these criteria:

$$\psi_1 = \sum_{k\neq 0} A_k \frac{\cosh ky}{\cosh k\Delta_1}\cos kx + A_0 + \frac{1}{2}C_1(t)y^2, \tag{66}$$

$$\psi_2 = \sum_{k\neq 0} B_k \frac{\cosh[k(L_y - y)]}{\cosh k\Delta_2} \cos kx + B_0 + \frac{1}{2}C_1(t)(L_y - y)^2, \quad (67)$$

where A_k and B_k are functions of time only, and $\Delta_2 = L_y - \Delta_1$. The constant factors $\cosh k\Delta_{1,2}$ are introduced in Eqs. (66) and (67) for convenience.

Now we have to match the solutions at the interface. In the linear approximation, it is sufficient to treat the interface as unperturbed. First, we use Eq. (63), which yields $A_k = B_k$ for $k \neq 0$, and

$$B_0 = A_0 + \frac{1}{2}C_1(t)\Delta_1^2 - \frac{1}{2}C_2(t)\Delta_2^2.$$

Second, we use relations (62). We calculate the normal velocity components v_{1n} and v_{2n} at the interface from Eqs. (61), (66), and (67), and express the interface curvature in the linear approximation as

$$\mathcal{K} \simeq \sum_{k\neq 0} k^2 \delta_k(t) \cos kx.$$

Now we calculate c_n:

$$c_n = \frac{d\delta(x,t)}{dt} = \dot{\delta}_0(t) + \sum_{k\neq 0} \dot{\delta}_k(t) \cos kx.$$

Then relations (62) yield the following equations:

$$u_1 \sum_{k\neq 0} A_k k \tanh(k\Delta_1) \cos kx + u_1 C_1(t)\Delta_1 = \dot{\delta}_0(t) + \sum_{k\neq 0} \dot{\delta}_k(t) \cos kx - g u_1 (P - P_*) + u_1 f \sum_{k\neq 0} k^2 \delta_k(t) \cos kx, \quad (68)$$

$$-u_2 \sum_{k\neq 0} A_k k \tanh(k\Delta_2) \cos kx - u_2 C_2(t)\Delta_2 = \dot{\delta}_0(t) + \sum_{k\neq 0} \dot{\delta}_k(t) \cos kx - g u_2 (P - P_*) + u_2 f \sum_{k\neq 0} k^2 \delta_k(t) \cos kx. \quad (69)$$

It is seen from Eqs. (68) and (69) that the volumetric mode $k = 0$ is decoupled from the deformation mode $k \neq 0$, and each mode can be considered separately. For the volumetric mode, Eqs. (68) and (69) reduce to

$$\Delta_1 \frac{\partial \ln u_1}{\partial P_*} \dot{P} - \dot{\delta}_0(t) + g u_1 (P - P_*) = 0, \quad (70)$$

$$-\Delta_2 \frac{\partial \ln u_2}{\partial P_*} \dot{P} - \dot{\delta}_0(t) + g u_2 (P - P_*) = 0. \quad (71)$$

Eliminating $\dot{\delta}_0(t)$, we obtain an equation for $\dot{P}$ which represents a one-dimensional form of Eq. (52) [and coincides with Eq. (37) of the paper AMS]. This is not surprising, as both the equilibrium interface and its volumetric perturbation are describable in this case by the one-dimensional theory. Equations (70) and (71) can be easily solved, and the results are the following:

$$\Delta P = \Delta P_0 \exp\left(-\frac{t}{\tau_1}\right), \quad (72)$$

$$\delta_0(t) = \Delta_0 + \Delta P_0 \frac{\Delta_1 u_2 \frac{\partial \ln u_1}{\partial P_*} + \Delta_2 u_1 \frac{\partial \ln u_2}{\partial P_*}}{u_2 - u_1} \times \left[\exp\left(-\frac{t}{\tau_1}\right) - 1\right], \quad (73)$$

where $\Delta P = P - P_*$, ΔP_0 and Δ_0 are the initial values of ΔP and δ_0, respectively, and

$$\tau_1 = -\frac{\Delta_1 \frac{\partial \ln u_1}{\partial P_*} + \Delta_2 \frac{\partial \ln u_2}{\partial P_*}}{g(u_2 - u_1)} \quad (74)$$

is the characteristic pressure relaxation time, predicted by the planar theory of AMS. Recall that $\tau_1 > 0$. Roughly speaking, τ_1 is of the order of the typical size of a pattern (in our scaled units), that is, much larger than unity (see AMS).

Therefore, for the volumetric perturbations, the small pressure perturbation goes to zero with time, P approaching P_*. Meanwhile, the interface relaxes, in general, to a new equilibrium position, which is close to the original one. It is clear that the volumetric mode must be neutrally stable if the initial pressure perturbation $\Delta P_0 = 0$, and we see from Eq. (73) that it is indeed the case.

Now let us consider the deformation modes. For such modes, the pressure perturbation vanishes, and we obtain from Eqs. (68) and (69) the following relations:

$$u_1 A k \tanh(k\Delta_1) - \dot{\delta}_k(t) - u_1 f k^2 \delta_k(t) = 0, \quad (75)$$

$$u_2 A k \tanh(k\Delta_2) + \dot{\delta}_k(t) + u_2 f k^2 \delta_k(t) = 0. \quad (76)$$

Looking for $\delta_k(t)$ in the form of

$$\delta_k(t) = \delta_k(0) \exp(qt),$$

we arrive at two homogeneous linear algebraic equations, whose solvability condition yields

$$q = -k^2 f u_1 u_2 \frac{\tanh(k\Delta_1) + \tanh(k\Delta_2)}{u_1 \tanh(k\Delta_1) + u_2 \tanh(k\Delta_2)}. \quad (77)$$

Recall that $k = \pi n/L_x, n = 1, 2, \ldots$.

Since the f factor is always positive, we have $q < 0$, that is, the interface is stable with respect to small deformations. The characteristic relaxation time $\tau_2 \sim q^{-1}$ is defined by the lowest-order mode $n = 1$. Roughly speaking, τ_2 is of the order of the *squared* size of the pattern, therefore $\tau_2 \gg \tau_1$.

It is instructive to look into two limiting cases of Eq. (77). In the case of $k\Delta_1, k\Delta_2 \to \infty$, we expect that the boundaries of the system do not play any role. Indeed, the damping rate q reduces to a "local" form

$$q = -2k^2 f \frac{u_1 u_2}{u_1 + u_2}, \tag{78}$$

and the specific volumes of the two phases enter the damping rate in a symmetric way.

In the case of $k\Delta_1 \to 0$ almost the entire domain Ω is occupied by the phase 2. Therefore one might expect that the damping rate will be determined by the parameters of the phase 2. In fact, the opposite is true, as the damping rate becomes

$$q = -k^2 f u_1,$$

and it is u_1 that determines the damping rate. Similarly, u_2 determines the damping rate in the case of $k\Delta_2 \to 0$, when the phase 1 dominates.

Let us summarize the main results of this subsection. An arbitrary small perturbation of the equilibrium interface in the slab geometry can be represented as a volumetric perturbation ($k = 0$), accompanied by a pressure variation, and a set of isobaric deformation perturbations with different $k \neq 0$. All these perturbations are damped independently. The volumetric perturbation relaxes on the time scale $\tau_1 \sim L \gg 1$, while the deformation perturbations (more precisely, their lowest modes) decay much more slowly, on the time scale $\tau_2 \sim L^2 \gg \tau_1$. Although we have solved the stability problem for two dimensions, the results are valid for three dimensions as well, because of the symmetry of the unperturbed state.

B. Shape stability of a perfect drop (bubble)

Now let us consider the stability of a single two-dimensional (circular) drop of radius R (region 1), which is in equilibrium with an ambient "vapor" (region 2). Now the equilibrium pressure P_{eq} differs from the area-rule value P_* by the correction $f/(gR)$, as predicted by Eq. (33). The results will be immediately extended to the case of a bubble (region 2), surrounded by "liquid" (region 1). The simplest problem is formulated for a circular domain Ω with a radius $L > R$, concentric with the drop. Similar to the previous problem, small volumetric (purely radial) perturbations of the drop, which are generally accompanied by a pressure perturbation, decouple from (isobaric) azimuthal perturbations of the drop interface. Therefore we shall consider the radial stability separately in the next subsection. Here we shall assume that the pressure perturbations are absent and specify a small interface perturbation in the form of the radius variation $R\delta(\phi, t) = R\delta_m(t) \sin m\phi$, where ϕ is the polar angle and $m = 1, 2, \ldots$. For the isobaric perturbations, Eqs. (39) and (61) yield the Laplace equation for the "potential" ψ in the regions 1 and 2. In the region 1, the solution can be written as

$$\psi_1 = A_1 r^m \sin m\phi, \tag{79}$$

while in the region 2

$$\psi_2 = \left(A_2 r^m + \frac{B_2}{r^m} \right) \sin m\phi, \tag{80}$$

where A_1, A_2 and B_2 are constants. The further procedure is almost identical to that of the previous subsection; therefore we can be quite brief. We have to zero $\partial\psi_2/\partial r$ at the boundary $r = L$, require $\psi_1 = \psi_2$ at the (unperturbed) interface $r = R$, and use relations (62). For the latter operation we need an expression for the curvature *perturbation*, as the leading curvature term, proportional to $1/R$, cancels out with the term proportional to $P_{eq} - P_*$. In the linear approximation, the curvature perturbation is

$$-\frac{1}{R}\left(\frac{\partial^2 \delta(\phi, t)}{\partial \phi^2} + \delta(\phi, t) \right) = \frac{1}{R}(m^2 - 1)\delta(\phi, t),$$

and relations (62) reduce to two algebraic equations for A_1 and $\delta_m(t)$:

$$Rq\delta_m(t) + \frac{fu_1}{R}(m^2 - 1)\delta_m(t) - u_1 m A_1 R^{m-1} = 0, \tag{81}$$

$$Rq\delta_m(t) + \frac{fu_2}{r}(m^2 - 1)\delta_m(t) - u_2 m A_1 R^{m-1} \frac{\xi^m - \xi^{-m}}{\xi^m + \xi^{-m}} = 0, \tag{82}$$

where $\xi = R/L$ and where we have put $\delta_m(t) = \hat{\delta} \exp(qt)$. From the solvability condition we find

$$q = -\frac{2f(m^2 - 1)u_1 u_2}{R^2 \left[u_1 + u_2 - (\frac{R}{L})^{2m}(u_2 - u_1) \right]} \qquad (m = 1, 2, \ldots) . \tag{83}$$

We see that the $m = 1$ mode is neutrally stable, as can be expected (it corresponds to a displacement of the drop as a whole). The azimuthal modes with $m > 1$ are always damped, so that the interface finally recovers its circular form. The characteristic relaxation time τ_2 is proportional to the squared radius of the drop, and therefore $\tau_2 \gg \tau_1$, as in the previous case of a planar interface. In the limit of a small drop, $R/L \to 0$, we have

$$q = -\frac{2f(m^2 - 1)u_1 u_2}{R^2(u_1 + u_2)}, \tag{84}$$

and this result must be independent of the form of the boundary. Alternatively, when $R/L \to 1$ (phase 1 dominates), the damping rate

$$q = -\frac{f(m^2 - 1)u_2}{R^2}$$

is determined by the phase 2 only.

The three-dimensional problem can be solved in a sim-

ilar way. We put a spherical drop in the center of a spherical cavity and prescribe a small perturbation of the drop shape, proportional to the spherical harmonic $Y_{lm}(\theta,\phi)$. We find that the perturbation is always damped, and the damping rate is the following:

$$q = -\frac{2f(l^2-1)(l+1)u_1u_2}{R^2[lu_1+(l+1)u_2+(l+1)(u_1-u_2)(R/L)^{2l+1}]} \qquad (l=1,2,\ldots)\ . \quad (85)$$

The results of this subsection can easily be reformulated for the problem of stability of an equilibrium bubble (phase 2) in the liquid (phase 1). The two- and three-dimensional damping rates in this case can be obtained by permutation of indices 1 and 2 in Eqs. (83) and (85).

Therefore individual drops and bubbles are stable with respect to deformation of their shapes, and the characteristic time for the restoration of their perfect form is $\tau_2 \sim R^2$.

C. Radial stability of a single drop (bubble)

Now we shall study the behavior of purely radial perturbations of a single drop which are accompanied by pressure variations. The linear theory of radial stability can be developed in a standard manner, if we employ Eq. (61), the linearized version of Eq. (39) for the regions 1 and 2, and matching conditions (62) and (63). More instructive, however, is a direct approach that we shall employ now. We shall use the (nonlinearized) super-reduced equations in the limit of $P - P_* \ll P_*$, so that it will be possible to go beyond the linear theory and consider large variations of the drop radius.

We begin with a two-dimensional problem. Consider a circular domain Ω, containing a circular "drop" of radius R, concentric with Ω, and surrounded by "vapor" (phase 2). Let $|\Omega| = S_0$ be the area of the domain Ω. As usual, we assume that the plasma pressure P is close to the area-rule value P_*: $P - P_* \ll P_*$. Let the drop radius and initial pressure be not in equilibrium, so that the system starts to evolve, P and R changing in time. Physically, mass and heat exchange between the drop and the vapor starts. Since the radial mode decouples from the (damped) azimuthal perturbations considered in the previous subsection, $P(t)$ and $R(t)$ represent the only variables of the problem, and we need two ordinary differential equations to describe the dynamics. An equation for $\dot{P}$ is provided by Eq. (52), where we just need to calculate $\langle\mathcal{K}\rangle, \langle L\rangle$ and $\langle u\rangle$, using the two-dimensional versions of Eqs. (53)–(56). The result is the following:

$$\dot{P} = \frac{2\left[g(P-P_*)-\frac{f}{R}\right][u_2(P_*)-u_1(P_*)]}{R\left[\frac{\partial \ln u_1}{\partial P_*}+\left(\frac{S_0}{\pi R^2}-1\right)\frac{\partial \ln u_2}{\partial P_*}\right]}\ . \qquad (86)$$

Now let us make use of the mass conservation in the system,

$$\frac{d}{dt}\left(\frac{\pi R^2}{u_1}+\frac{S_0-\pi R^2}{u_2}\right)=0. \qquad (87)$$

After differentiation and linearization around P_*, we have

$$\frac{2\pi R\dot{R}}{u_1(P_*)}-\frac{\pi R^2}{u_1(P_*)}\frac{\partial \ln u_1}{\partial P_*}\dot{P}-\frac{2\pi R\dot{R}}{u_2(P_*)} -\frac{S_0-\pi R^2}{u_2(P_*)}\frac{\partial \ln u_2}{\partial P_*}\dot{P}=0. \qquad (88)$$

Substituting for $\dot{P}$ its value from Eq. (86) we obtain after some algebra the second evolution equation:

$$\dot{R} = \frac{u_1u_2\left[g(P-P_*)-\frac{f}{R}\right]\left[\frac{1}{u_1}\frac{\partial \ln u_1}{\partial P_*}+\left(\frac{S_0}{\pi R^2}-1\right)\frac{1}{u_2}\frac{\partial \ln u_2}{\partial P_*}\right]}{\frac{\partial \ln u_1}{\partial P_*}+\left(\frac{S_0}{\pi R^2}-1\right)\frac{\partial \ln u_2}{\partial P_*}}, \qquad (89)$$

where $u_{1,2} = u_{1,2}(P_*)$. Equations (86) and (89) can be integrated analytically in the general case. However, we shall limit ourselves to the important case of a relatively small drop: $\pi R^2 \ll S_0$. One can expect that the results obtained in this case will be valid for an *arbitrary* form of the boundary Γ (unless the drop is located too close to the boundary), as the boundary-induced deformations of the drop shape are small here. Using the small parameter $\pi R^2/S_0$ and assuming that neither $u_{1,2}$, nor their P derivatives introduce large or small parameters, we obtain a less cumbersome set of equations:

$$\dot{P} = \frac{2\pi u_2(u_2-u_1)R}{S_0\frac{\partial u_2}{\partial P}}\left[g(P-P_*)-\frac{f}{R}\right], \qquad (90)$$

$$\dot{R} = u_1\left[g(P-P_*)-\frac{f}{R}\right]. \qquad (91)$$

The first integral of this system is

$$P-\frac{\pi u_2(u_2-u_1)R^2}{S_0u_1\frac{\partial u_2}{\partial P}} = \text{const}, \qquad (92)$$

so that the integral curves on the phase plane (R,P) represent descending quadratic parabolas (recall that $\partial u_{1,2}/\partial P < 0$). Because of the smallness of $\pi R^2/S_0$, the parabolas descend slowly.

In the limit of $S_0 \to \infty$ the parabolas reduce to straight lines parallel to the R axis (the pressure becomes constant). In this case there is a constant "critical" drop radius,

$$R_c = \frac{f}{g(P-P_*)},$$

so that the drop with $R = R_c$ is in equilibrium, as pre-

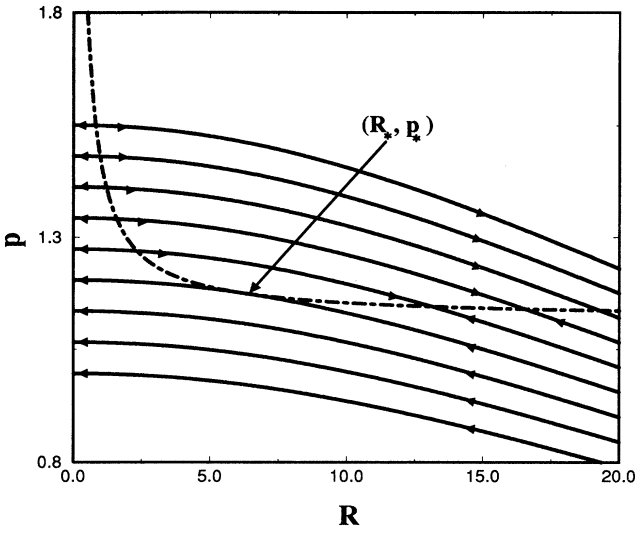

FIG. 2. The phase plane of Eqs. (90) and (91), describing the dynamics of radial perturbations of a single drop. Solid lines are the integral curves (92), dashed line is the line of equilibria. The numerical values correspond to a specific choice of the heating-cooling function and parameters of the problem.

dicted in Sec. III. This equilibrium is, however, unstable: a drop with $R > R_c$ grows with time, approaching the linear law $R \sim t$, while a drop with $R < R_c$ shrinks and disappears in a finite time. At this stage we notice a clear analogy between this problem and various problems of growth of droplets in first-order phase transitions, where capillarity introduces mathematically similar curvature-dependent effects.

Let us return to the case of a large but finite S_0. The system (90) and (91) [as well as its more general version (86) and (89)] possesses a "fixed line," or line of equilibria

$$g(P - P_*) - \frac{f}{R} = 0,$$

which gives a family of equilibrium pressure values $P_{eq}(R)$ [or a family of the critical radii $R_c(P)$]. We see that, for any initial condition $R(0), P(0)$, the dynamics is determined by the relative position of the corresponding integral curve and the line of equilibria.

Figure 2 shows the structure of the phase plane. The solid lines are the integral curves (92), while the dashed line is the line of equilibria. For initial conditions lying on those integral curves, which do not intersect the line of equilibria, the drop will never reach an equilibrium. One can see that it will shrink and disappear in a finite time. (Actually, the theory breaks down for small drop radii. However, our numerical simulations, free from this limitation, will show that the drop evaporation indeed persists until the drop disappears.)

Now consider integral curves, which have two intersection points with the line of equilibria. These points represent two equilibria, the first with a smaller and the second with a larger drop radius. It is easy to see that the smaller-radius equilibrium is always unstable, so that the drop either shrinks and disappears, or expands until a new equilibrium with a larger drop radius is reached.

Therefore, the line of equilibria consists of two parts, unstable and stable. The stability border, dividing the line of equilibria into these two parts, is the tangency point between the line of equilibria and an integral curve. This point can be easily found, and it gives the minimum value R_* of the stable drop radius:

$$R_* = \left[-\frac{f u_1 S_0 \frac{\partial u_2}{\partial P}}{2\pi g u_2 (u_2 - u_1)} \right]^{1/3}. \tag{93}$$

We see that, while the minimum area of a stable drop, πR_*^2, increases with S_0 as $S_0^{2/3}$, its relative value $\pi R_*^2 / S_0$ decreases as $S_0^{-1/3}$.

Equation (93) can also be obtained from linear stability analysis. Indeed, linearizing Eqs. (90) and (91) around a point (R_0, P_0), lying on the line of equilibria $P_{eq}(R)$, one can easily obtain the following growth or damping rate for small perturbations δR and δP:

$$q = \frac{2\pi g u_2 (u_2 - u_1) R_0}{S_0 \frac{\partial u_2}{\partial P}} + \frac{f u_1}{R_0^2}. \tag{94}$$

The marginal stability condition $q = 0$ immediately gives Eq. (93). Equation (94) is quite instructive, as it predicts the characteristic time scales for the growth or damping of the small perturbations. Close to the marginal stability, the characteristic time goes to infinity. On the stable part of the line of equilibria, far from the marginal stability, the characteristic time of relaxation to equilibrium is quite large, as it is proportional to a large factor S_0/R_0. In contrast, the characteristic time scale of the initial (linear) growth of an unstable drop (also far from the marginal stability) is proportional to R_0^2 and independent of the area S_0.

The three-dimensional problem of the radial stability of a single drop can be analyzed similarly. As we shall need these results in the following section, we present them in some detail. Let us consider an arbitrary three-dimensional domain with the volume V_0, containing a spherical drop of radius R surrounded by "vapor" (phase 2). The drop volume $(4\pi/3)R^3$ is much less than V_0. In this case, the coupled equations for $\dot{P}$ and $\dot{R}$ are the following:

$$\dot{P} = \frac{4\pi u_2 (u_2 - u_1) R}{V_0 \frac{\partial u_2}{\partial P}} \left[g(P - P_*) - \frac{2f}{R} \right], \tag{95}$$

$$\dot{R} = u_1 \left[g(P - P_*) - \frac{2f}{R} \right]. \tag{96}$$

The first integral,

$$P - \frac{4\pi u_2 (u_2 - u_1) R^3}{3 V_0 u_1 \frac{\partial u_2}{\partial P}} = \text{const}, \tag{97}$$

describes a family of slowly descending cubic parabolas. The phase portrait is similar to that shown in Fig. 2, and the dynamics is the same as in two dimensions. In

particular, the line of equilibria

$$g(P-P_*)-\frac{2f}{R}=0$$

consists of two parts, unstable and stable. The stability border is

$$R_*=\left[-\frac{fu_1V_0\frac{\partial u_2}{\partial P}}{2\pi g u_2(u_2-u_1)}\right]^{1/4}, \tag{98}$$

so that the minimum volume of a stable drop grows with V_0 as $V_0^{3/4}$, while the relative volume decreases as $V_0^{-1/4}$.

Finally, radial stability of a bubble (phase 2) in the "liquid" (phase 1) can be considered in the same way. The results can be obtained from those for the drop by permutating indices and changing the sign inside the square brackets. For example, the minimum radius of a stable bubble in three dimensions is the following:

$$R_*=\left[-\frac{fu_2V_0\frac{\partial u_1}{\partial P}}{2\pi g u_1(u_2-u_1)}\right]^{1/4}. \tag{99}$$

Therefore we have found that an individual equilibrium drop (bubble) can be either stable or unstable, and found the instability criterion. An unstable drop (bubble) either shrinks and disappears in a finite time, or expands until a stable equilibrium is reached [33]. More generally, the phase portrait analysis enabled us to follow the dynamics of an arbitrary nonequilibrium drop (under the condition $P-P_* \ll 1$) and reach the same conclusions.

VI. INTERACTION BETWEEN DROPS (BUBBLES): OSTWALD RIPENING

Let us consider interaction between $N \geq 2$ drops or bubbles. As usual, we assume that $\Delta P \ll P_*$. Also, we assume that the drop radii are large enough, $R_i \gg 1$, $i=1,2,...,N$, so that our weak curvature theory is valid, and that the distances between the drops and the boundary and between the drops themselves are much larger than the drop radii. The latter condition implies that the total area occupied by the drops is relatively small: $S_0 \gg \pi\sum_{i=1}^N R_i^2$. In this small volume fraction limit, the drop-drop interaction results solely from the (uniform) pressure variations in time. Indeed, any deviation from the equilibrium pressure $P_{eq}(R_i)$ leads to heat and mass exchange between the drops and the "vapor," which results in a nonlocal heat and mass exchange between the drops. The pressure "mismatch" $P-P_*$ can be viewed as the "mean field" of the model. In particular, this interaction will mainly cause radial variations of the drops, while their shape deformations will be small. As we have already seen in Sec. III, the interaction vanishes in equilibrium, when all the drops have the same radius. However, this equilibrium will be found to be unstable with respect to small variations of the drop radii. Therefore our aim will be to describe the dynamics of this system and its relaxation to the final state. In Sec. VI A we deal with the dynamic behavior of N drops. In Sec. VI B we employ and partially revise the theory of Lifshitz and Slezov [34] and Wagner [35] to find a family of "universal" distribution functions of large ensembles of drops with respect to their radii.

A. Many drops' dynamics: Ostwald ripening

Let us start with the two-dimensional case. According to Eq. (49), the radial mass outflow from each drop is

$$j_i=-g(P-P_*)+\frac{f}{R_i}, \quad i=1,2,...,N \tag{100}$$

(negative outflow means inflow). Multiplying j_i by the drop circumference $2\pi R_i$, we obtain the mass loss rate of each drop:

$$\dot{M}_i=-2\pi j_i R_i=\frac{d}{dt}\left(\frac{\pi R_i^2}{u_1}\right). \tag{101}$$

On the other hand, the total mass in the system is preserved:

$$\frac{d}{dt}\left(\sum_{i=1}^N\frac{\pi R_i^2}{u_1}+\frac{S_0-\pi\sum_{i=1}^N R_i^2}{u_2}\right)=0. \tag{102}$$

After taking the time derivatives in Eqs. (101) and (102), we solve the resulting equations for $\dot{P}$ and $\dot{R}_i$. In the limit of $S_0 \gg \pi\sum_{i=1}^N R_i^2$, we arrive at

$$\dot{P}=\frac{2\pi u_2(u_2-u_1)}{S_0\frac{\partial u_2}{\partial P}}\left[g(P-P_*)\sum_{i=1}^N R_i-fN\right], \tag{103}$$

$$\dot{R}_i=u_1\left[g(P-P_*)-\frac{f}{R_i}\right], \quad i=1,2,...,N, \tag{104}$$

where $u_{1,2}=u_{1,2}(P_*)$. These equations directly generalize Eqs. (90) and (91), obtained for $N=1$. Equations (103) and (104) possess the first integral

$$P-\frac{\pi u_2(u_2-u_1)}{S_0u_1\frac{\partial u_2}{\partial P}}\sum_{i=1}^N R_i^2=\text{const}; \tag{105}$$

however, it is not enough to solve the $(N+1)$-dimensional problem.

In three dimensions, the corresponding equations are the following:

$$\dot{P}=\frac{4\pi u_2(u_2-u_1)}{V_0\frac{\partial u_2}{\partial P}}\left[g(P-P_*)\sum_{i=1}^N R_i^2-2f\sum_{i=1}^N R_i\right], \tag{106}$$

$$\dot{R}_i=u_1\left[g(P-P_*)-\frac{2f}{R_i}\right], \quad i=1,2,...,N, \tag{107}$$

where it is assumed that $V_0 \gg (4/3)\pi \sum_{i=1}^{N} R_i^3$. The corresponding first integral is

$$P - \frac{4\pi u_2(u_2-u_1)}{3V_0 u_1 \frac{\partial u_2}{\partial P}} \sum_{i=1}^{N} R_i^3 = \text{const.} \tag{108}$$

Let us normalize Eqs. (103) and (104), and, correspondingly, Eqs. (106) and (107) in the following way. Introduce a new time $\tau = (d-1)u_1 f t$ and pressure

$$\Delta p = \frac{g(P-P_*)}{f(d-1)}$$

(recall that $d = 2$ and 3 for two and three dimensions, respectively). Then we can rewrite Eqs. (103)–(105) as

$$\frac{d\Delta p}{d\tau} = -\epsilon \left(p \sum_{i=1}^{N} R_i - N \right), \tag{109}$$

$$\frac{dR_i}{d\tau} = \Delta p - \frac{1}{R_i}, \quad i = 1, 2, ..., N, \tag{110}$$

and

$$\Delta p + \frac{\epsilon}{2} \sum_{i=1}^{N} R_i^2 = \text{const}, \tag{111}$$

while Eqs. (106)–(108) are rewritten as

$$\frac{d\Delta p}{d\tau} = -\epsilon \left(\Delta p \sum_{i=1}^{N} R_i^2 - \sum_{i=1}^{N} R_i \right), \tag{112}$$

$$\frac{dR_i}{d\tau} = \Delta p - \frac{1}{R_i}, \quad i = 1, 2, ..., N, \tag{113}$$

and

$$\Delta p + \frac{\epsilon}{3} \sum_{i=1}^{N} R_i^3 = \text{const}, \tag{114}$$

where

$$\epsilon = -\frac{2\pi g u_2(u_2-u_1)}{f S_0 u_1 \frac{\partial u_2}{\partial P}} > 0$$

for the two-dimensional case, and

$$\epsilon = -\frac{2\pi g u_2(u_2-u_1)}{f V_0 u_1 \frac{\partial u_2}{\partial P}} > 0$$

for three dimensions. Note that the scaled equations for $\dot{R}_i$ look the same in both cases.

Both the two- and the three-dimensional systems have simple equilibria $R_i = R_0$ (that is, N identical drops) and $\Delta p = 1/R_0$, which are unstable with respect to small variations of the drop radii. Indeed, let δR_k and δR_j be small perturbations of the radii of the kth and jth drops, respectively. Linearizing Eq. (110) or (113) for the drops k and j around equilibrium, and subtracting one from another, we obtain

$$\frac{d}{d\tau}(\delta R_k - \delta R_j) = \frac{1}{R_0^2}(\delta R_k - \delta R_j). \tag{115}$$

One can see that a small difference in *any* two drops' radii will grow exponentially in time. The characteristic growth time (in the "old" units of time) coincides with the growth time for a single, radially unstable drop far from the instability threshold [see, for example, Eq. (94) for two dimensions]. Furthermore, the growth of the difference in the radii of *any* two drops in time persists far from equilibrium. Indeed, subtracting the j-th equation (110) [or (113)] from the kth equation, we arrive at

$$\frac{d}{d\tau}(R_k - R_j) = \frac{R_k - R_j}{R_k R_j}$$

so that $|R_k - R_j|$ grows monotonically in time. As a consequence, the initial ordering of the drop radii (let it be $R_1 < R_2 < \cdots < R_N$) persists. On the other hand, the total area (correspondingly, the total volume), occupied by the drops is always finite. (This can be easily seen if we express the time derivative of the total area, using Eqs. (110) and (111) [correspondingly, Eq. (113) and (114)].) It follows that *at least* one drop must be shrinking. Preservation of the size ordering in the process of interaction means that it is the smallest drop, that is, drop 1, whose radius first reaches zero. It is important that this singularity develops in a finite time, so that the smallest drop disappears, and the number of drops becomes $N-1$. At this stage (after the singularity), we have to redefine the "initial conditions" and the first integral, then employ the same arguments, and so on.

Therefore the dynamics of an ensemble of drops proceeds as a "harsh" competition mediated by the time-dependent pressure of the system. The smallest drop shrinks and disappears first. Then goes the second smallest drop, etc. The process continues until only one drop (the largest) remains [36]. The same result is valid for an ensemble of N bubbles. This type of dynamics, when larger drops thrive at the expense of smaller ones, is known in the dynamics of first-order phase transitions as Ostwald ripening [37].

B. Many drops' statistics: universal scalings and self-similar distributions

Now let us assume that a large number of drops, $N \gg 1$, has developed in the earlier conductive stage. Then we can introduce the (time-dependent) distribution function of the drops with respect to their radii, $F(R,\tau)$. Consider the three-dimensional geometry. By definition, $\int_0^\infty F(R,\tau)dR = n(\tau)$, where $n(\tau)$, the number of drops per unit volume, is a continuous function of the scaled time τ.

The distribution function must satisfy the continuity equation in the space of radii,

$$\frac{\partial F}{\partial \tau} + \frac{\partial}{\partial R}(\dot{R}F) = 0, \quad \dot{R} = \Delta p - \frac{1}{R}. \tag{116}$$

The first integral (114) can be rewritten as

$$\Delta p + \frac{\epsilon_0}{3}\int_0^\infty R^3 F(R,\tau)dR = Q = \text{const}, \qquad (117)$$

where

$$\epsilon_0 = -\frac{2\pi g u_2(u_2-u_1)}{f u_1 \frac{\partial u_2}{\partial P}} > 0.$$

Equations (116) and (117) represent a closed set. Given the initial conditions $F(R,0)$ and $\Delta p(0)$, they determine the whole evolution of the system up to the times when the number of drops becomes small, and the statistical description fails. In this formulation the problem is very similar mathematically to the classical problem of the kinetics of diffusive decomposition of supersaturated solid solutions, studied in the pioneering work by Lifshitz and Slezov [34]. The main difference lies in the expression for $\dot{R}$, which in their case included an additional factor $1/R$. The general approach of Lifshitz and Slezov was adopted in many other systems showing Ostwald ripening (for a recent bibliography on Ostwald ripening theory, including an account of the volume fraction effects, see [38–42]). Among them, Wagner [35] was the first to consider a diffusively decomposing system with a chemical reaction on the interphase surface. It appears that the corresponding (scaled) equations of Wagner exactly coincide with our Eqs. (116) and (117). Therefore we will be quite brief in presenting the results, except those which differ from those of Wagner.

The theory of Lifshitz and Slezov predicts that, for sufficiently large times, any extended distribution function of the drops with respect to their radii approaches a universal self-similar form, which represents an intermediate asymptotics of the problem. For our system, the general self-similar distribution function is $F(R,\tau) = \tau^{-2}\Phi(R/\tau^{1/2})$ [43], while the scaled pressure mismatch Δp decreases as $\beta\tau^{-1/2}$. This implies that the "drop concentration" n decreases as $\eta\tau^{-3/2}$, while the average drop radius

$$\bar{R} = \frac{\int_0^\infty RF(R,\tau)dR}{\int_0^\infty F(R,\tau)dR}$$

grows as $\chi\tau^{1/2}$. The positive coefficients η, χ, and β are uniquely determined by the function $\Phi(\xi)$:

$$\eta = \int_0^\infty \Phi(\xi)d\xi, \quad \chi = \frac{\int_0^\infty \xi\Phi(\xi)d\xi}{\int_0^\infty \Phi(\xi)d\xi},$$

$$\text{and} \quad \beta = \frac{\int_0^\infty \xi\Phi(\xi)d\xi}{\int_0^\infty \xi^2\Phi(\xi)d\xi}.$$

The function Φ satisfies an ordinary differential equation of the first order and a normalization condition, which one obtains from Eqs. (116) and (117). As the relative contribution of the pressure mismatch in the conservation law (117) goes to zero for large times, the normalization condition requires simply that the total volume occupied by the drops be preserved, which leads to

$$\int_0^\infty \xi^3\Phi(\xi)d\xi = \frac{3Q}{\epsilon_0}. \qquad (118)$$

The differential equation for Φ can be integrated by separation of variables, and we arrive at the following expression:

$$\Phi(\xi) = \text{const} \times \xi|\xi^2 - 2\beta\xi + 2|^{-5/2} \times \exp\left(-3\beta\int^\xi \frac{d\xi}{\xi^2 - 2\beta\xi + 2}\right). \qquad (119)$$

Further calculations depend on the number of real roots of the quadratic polynomial entering the integrand's denominator. If $0 < \beta < \sqrt{2}$, it has none. In this case $\Phi(\xi)$ from Eq. (119) is extended (that is, exists on the whole interval $0 < \xi < \infty$) and falls as ξ^{-4} as $\xi \to \infty$. It follows that the normalization integral (118) diverges logarithmically, which rules out this case.

In the special case of $\beta = \sqrt{2}$ (two equal roots, $\xi_1 = \xi_2 = \sqrt{2}$), we arrive at the solution found by Wagner [35]:

$$\Phi(\xi) = \text{const} \times \xi(\sqrt{2} - \xi)^{-5}\exp\left(-\frac{3\sqrt{2}}{\sqrt{2}-\xi}\right) \qquad (120)$$

for $\xi < \sqrt{2}$, and $\Phi(\xi) = 0$ elsewhere. The constant is determined by the normalization condition (118). This solution vanishes at $\xi = \sqrt{2}$ together with all its derivatives. For the Wagner solution we have $\chi = (8/9)\sqrt{2}$. Extending the arguments of Lifshitz and Slezov [34,44] to this case, one can assume that this particular solution will be the attractor of any *extended* initial distribution.

Now let us proceed to the case of $\beta > \sqrt{2}$, when the polynomial has two different real roots,

$$\xi_1 = \beta - \sqrt{\beta^2 - 2}, \quad \xi_2 = \beta + \sqrt{\beta^2 - 2},$$

both of them positive. Formal integration in Eq. (119) yields

$$\Phi(\xi) = \text{const} \times \xi|\xi_1 - \xi|^{-\frac{5}{2} + \frac{3\beta}{2\sqrt{\beta^2-2}}}|\xi_2 - \xi|^{-\frac{5}{2} - \frac{3\beta}{2\sqrt{\beta^2-2}}}. \qquad (121)$$

We can easily construct a positive, nonsingular solution, if we use Eq. (121) on the interval $(0,\xi_1)$ and put $\Phi(\xi) = 0$ for $\xi \geq \xi_1$. The condition $\Phi(\xi_1) = 0$ requires that $\beta < 5\sqrt{2}/4$ (otherwise, Φ diverges at $\xi = \xi_1$) [45]. Therefore we arrive at a one-parametric family of self-similar distribution functions. The whole family is defined on a quite narrow interval of the parameter β, $\sqrt{2} \leq \beta < 5\sqrt{2}/4$, the left boundary of which corresponds to the Wagner solution. The distribution functions (121) vanish at $\xi = \xi_1$, but their derivatives are generally nonzero there. These solutions were missed by Wagner. (Similar localized distributions can be constructed in the problem of Lifshitz and Slezov [34] as well, as was shown by Brown [46].)

Notice that the exponents of the power laws of the pressure mismatch, drop concentration, and average drop

radius as functions of time are independent of β. However, the coefficients β, η, and χ in the corresponding power laws (and, of course, the shape of the distribution function) vary with β. An important question is which of these self-similar distributions will actually develop, if one starts from a prescribed initial distribution. As suggested above, it is the Wagner solution which finally sets in for an extended initial condition. The case of localized initial conditions requires an additional analysis and will be addressed elsewhere. (Similar questions of the realizability of different self-similar solutions have arisen recently for the Lifshitz-Slezov case, where they are the object of much controversy [40,41].) It is important to recall that, no matter what the precise form of the "intermediate" self-similar solution is, the final state of the dynamics must be a single drop (bubble), as shown in Sec. VI A.

VII. NUMERICAL SIMULATIONS

The aim of our two-dimensional numerical simulations was to substantiate the "super-reduced" conductive relaxation model and verify some of the analytical results presented in the previous sections. We worked with the reduced model, described by Eqs. (22)–(24) and (26) and the boundary conditions (8) and (25). However, instead of the Euler equation (23) we employed the following much simpler equation for the velocity field:

$$\mathbf{v} = u\nabla\psi. \tag{122}$$

As has been shown in Sec. IV, this relation becomes accurate close to equilibrium. Essentially, we arbitrarily extend it to the whole dynamics. [It appears, however, that the front-curvature-dominated dynamics is quite insensitive to the details of the velocity field. For example, when instead of Eq. (122) we used a purely potential flow, $\mathbf{v} = \nabla\psi$, the results looked qualitatively the same.]

We found it convenient to rewrite the continuity equation (22) as a parabolic equation for u, expressing $\nabla \cdot \mathbf{v}$ from Eq. (24) and using Eq. (122):

$$\frac{\partial u}{\partial t} = u\left[\nabla^2 u - \lambda(u,P) - \frac{\dot{P}}{\gamma P} - \nabla\psi\nabla u\right] \tag{123}$$

where we put $\alpha = 0$. Using again Eqs. (22) and (122), we obtain a Poisson equation for ψ:

$$\nabla^2\psi = -\frac{\partial(u^{-1})}{\partial t}. \tag{124}$$

Finally, the global pressure equation (26) becomes

$$\frac{\dot{P}}{\gamma P} = -\frac{1}{L^2}\int_0^L\int_0^L \lambda(u,P)\,dx\,dy. \tag{125}$$

Equations (123)–(125) were solved in a square domain $L \times L$ with no-flux boundary conditions (in one case we employed periodical boundary conditions; see below). We varied L from 35 to 60, so that L was always much larger than the conductive Field length (that is, unity in the scaled variables). We put $\gamma = 5/3$, and employed a simple bistable heating-cooling function from AMS:

$$\lambda(u,P) = [u - u_1(P)][u - u_u(P)][u - u_2(P)] \tag{126}$$

with $u_1 = 1/(2P), u_u = P$, and $u_2 = 2/P$. In this case, the area-rule value of the pressure is $P_* = \sqrt{5}/2 \simeq 1.118$, while $g = 2\sqrt{2} \simeq 2.828$ and $f = 1$.

The differential operators entering Eq. (123) were evaluated by the pseudospectral method using a fast Fourier transform. We employed a split-step method, extracting an "effective" linear part of the differential operator in the right-hand side (RHS) of Eq. (123):

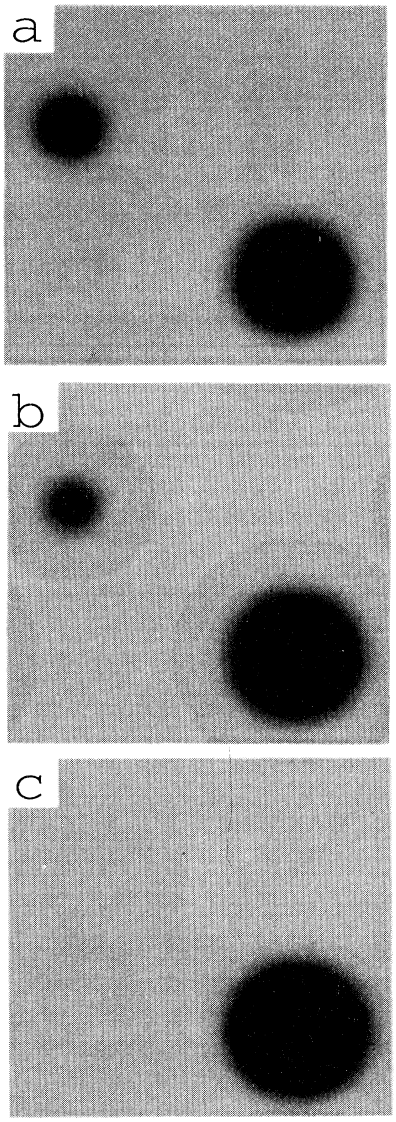

FIG. 3. Background-mediated competition between two drops, studied numerically. We started with two drops ($u = u_1$) in the "vapor" ($u = u_2$) for the initial pressure 1.2. The dimensions of the system are 60×60. Shown are the specific volume contours at $t = 5$ (a), 45 (b), and 100 (c).

$$\frac{\partial u}{\partial t} = u_c \nabla^2 u + (u - u_c)\nabla^2 u - u\left[\lambda(u, P) + \frac{\dot{P}}{\gamma P} - \nabla\psi\nabla u\right] \quad (127)$$

with $u_c = (u_1 + u_2)/2$. For the diffusion operator $u_c\nabla^2 u$ we used the exact analytical solution, while the remaining, nonlinear part of the RHS was calculated approximately. We performed the calculations on the square grid 256×256.

The values of u were updated according to the following algorithm:

$$u(t+\tau) = \exp\left[\frac{\tau}{2} f(t)\right] \exp(\tau u_c \nabla^2) \exp\left[\frac{\tau}{2} f(t)\right] u(t), \quad (128)$$

where

$$f(t) = \left[1 - \frac{u_c}{u(t)}\right] \nabla^2 u(t) - \lambda\left[u(t), P\right] + \frac{\dot{P}(t)}{\gamma P(t)} - \nabla\psi(t)\nabla u(t).$$

The operator $\exp(\tau u_c \nabla^2)$ was evaluated in the Fourier space. Equations (124) and (125) were solved at each time step using the values of $u(t)$ and $P(t)$ from the previous time step.

This numerical code turned out to be quite accurate, stable, and economical. At each time step we monitored the accuracy by checking the mass conservation

$$M = \int_0^L \int_0^L u^{-1}\, dx\, dy = \text{const}.$$

In all our runs this integral was preserved up to the third decimal place.

In all simulations we started from some density profile and a zero velocity. In the test simulations (not shown here), we started from a single drop of a moderate size (a few times smaller than the size of the domain Ω, but

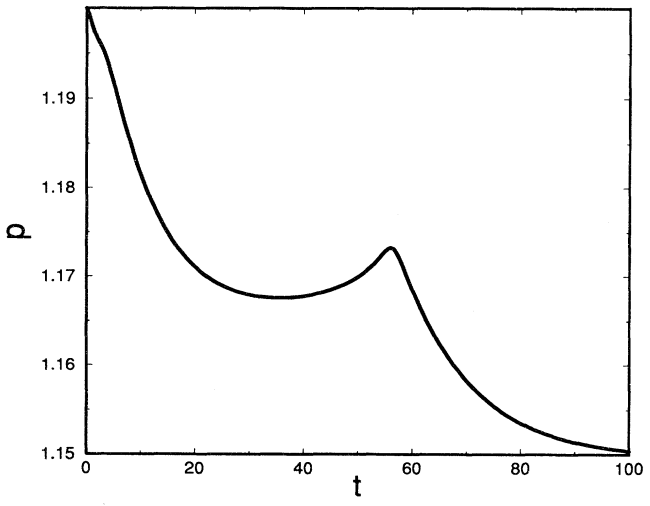

FIG. 4. Background-mediated competition between two drops, studied numerically. Shown is the pressure history for the same run as in Fig. 3. The peak at $t \simeq 57$ corresponds to the time moment of the disappearance of the smaller drop. The pressure finally approaches 1.15, which agrees with the surviving drop's radius in Fig. 3(c).

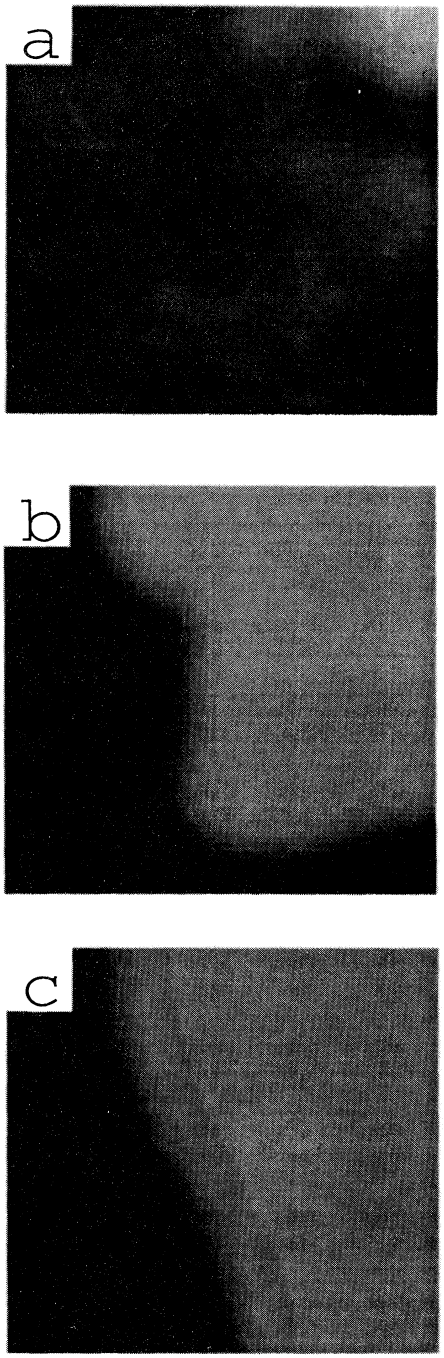

FIG. 5. Slab-type equilibrium, developing from a broadband noise. We started from a small-amplitude multimode perturbation of u around $u_0 = 0.9$. The initial pressure is 1.0; the dimensions of the system are 40×40. Shown are the specific volume contours at $t = 10$ (a), 20 (b), and 250 (c).

a few times larger than the conductive Field length) and were able to verify the analysis of the radial stability of a single drop presented in Sec. V C. We checked the main results described by Eqs. (90) and (91) [including the minimum radius of a stable drop, Eq. (93)] and found that these equations indeed describe the dynamics with a good accuracy.

Further simulations concerned the dynamics of a system of two or more drops with different radii. The results of Sec. VI A predict background-mediated competition between the drops and survival of the larger one. Figures 3 and 4 show the two drop dynamics, obtained numerically. (In these simulations we employed periodical boundary conditions.) It is seen from Figs. 3(a)–3(c) that the smaller drop shrinks and disappears as predicted, the larger drop and "vapor" thriving at its expense. Figure 4 shows the corresponding pressure history. The pressure is falling in the beginning, shows a pronounced peak close to the moment of the smaller drop disappearance, and finally approaches 1.15. Calculating the equilibrium radius R_{eq} from the relation

$$g(P - P_*) - \frac{f}{R} = 0,$$

we obtain $R_{eq} \simeq 11$, which is quite close to the visible radius of the drop in Fig. 3(c) (note that $L = 60$ in this run). Noticeable in Fig. 3 is an almost ideal preservation of the circular form of the drops which justifies the assumption of a purely radial interaction of the drops used in Sec. VI A. In a separate simulation (not shown here), we started with three drops of different radii and observed shrinkage and disappearance of the smallest one, followed by shrinkage of the next smallest.

In the next series of runs (Figs. 5–8), we started from a broadband "noise:" a small-amplitude multimode perturbation $\delta u(x, y)$ around a uniform state u_0. To develop radiative segregation, the value of u_0 must be somewhere between u_1 and u_2, and not too close to them. In the beginning (stages 1 to 3 of the dynamics), the results always look similar to the one-dimensional case (see AMS). First,

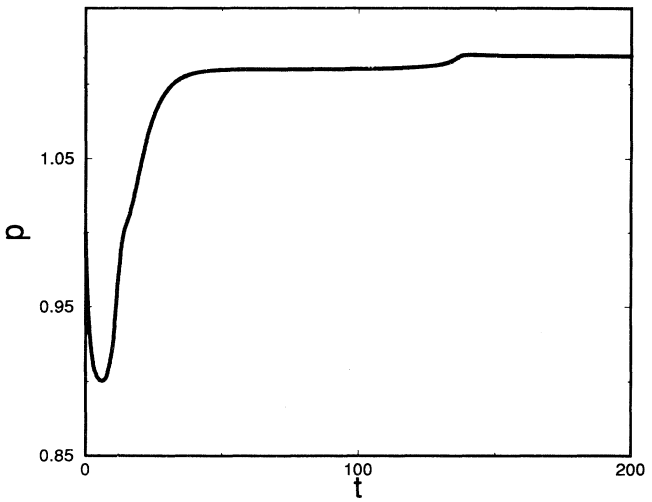

FIG. 6. Slab-type equilibrium, developing from a broadband noise. Shown is the pressure history for the same run as in Fig. 5. The pressure first jumps to 0.9 (so that the RCI starts to develop) and finally approaches the area-rule value $P_* = 1.118$.

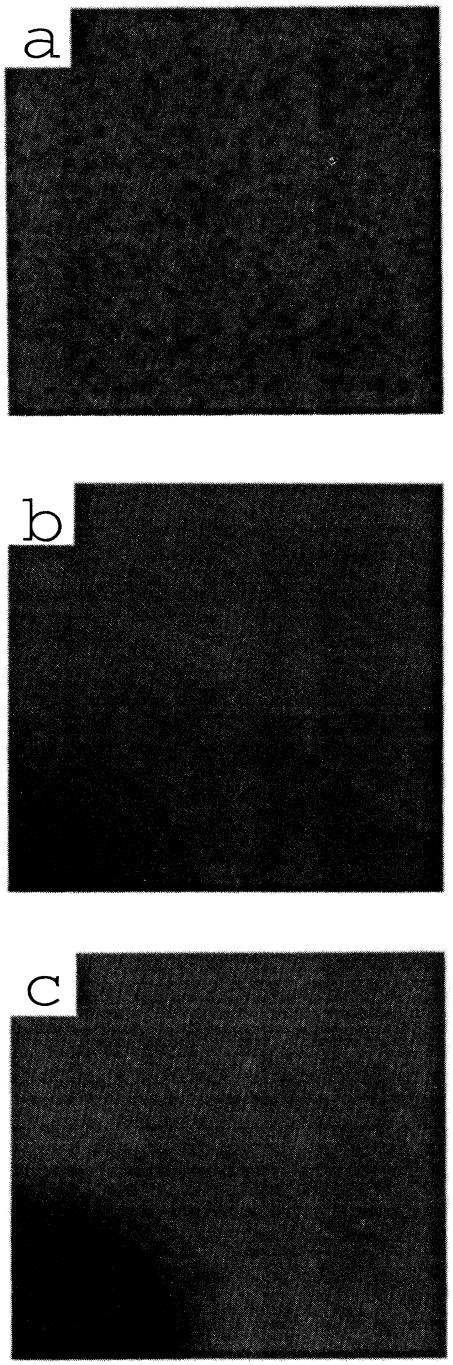

FIG. 7. Drop-type equilibrium, developing from a broadband noise. We started from a small-amplitude multimode perturbation of u around $u_0 = 1.4$. The initial pressure is 1.2, the dimensions of the system are 35×35. Shown are the specific volume contours at $t = 0$ (a), 20 (b), and 180 (c).

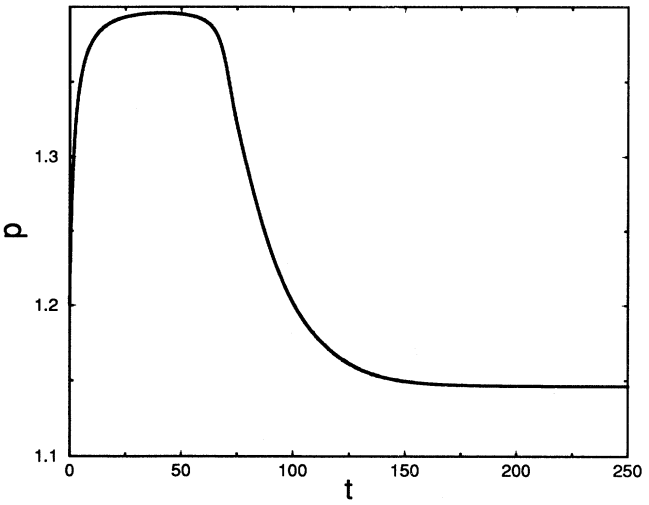

FIG. 8. Drop-type equilibrium, developing from a broad-band noise. Shown is the pressure history for the same run as in Fig. 7. The pressure first jumps close to 1.4 (so that the RCI starts to develop) and finally approaches the value, corresponding to the equilibrium radius of the forming drop.

the pressure "jumps" to u_0, so that u_0 quickly *becomes* an unstable equilibrium (stage 1). Then the linear stage of the RCI develops (stage 2), when the pressure is almost constant. Perturbations with too short wavelengths are strongly damped [see Eq. (7)], and they are already absent after a few units of time. In stage 3, strong plasma segregation develops: higher-density, cooler regions are formed (phase 1), which are surrounded by lower-density, hotter regions (phase 2).

We found that the subsequent evolution of the forming patterns proceeds in two different ways (depending on the initial conditions), and it has no analogs in one-dimensional theory. In Figs. 5 and 6, where we started from $u_0 = 0.9$, straightening of the interface between the phases 1 and 2 occurs, and a slab-type equilibrium develops. Figure 6 shows that the pressure approaches $P_* \simeq 1.118$ in complete agreement with our theory. Also, the final stage of this straightening is described by the linearized theory of Sec. V A. In Fig. 5(c), one can still see a slightly deformed interface, and the deformation mode is the fundamental, $n = 1$. By this time the shorter-wavelength modes $n = 2, 3, \ldots$ have already disappeared, as their damping rates (77) are 4, 9,... times higher.

In contrast, Figs. 7 and 8 (where we started from $u_0 = 1.4$) show the process of formation of a single equilibrium circular drop. [Actually, Fig. 7(c) shows a quarter of a drop, a compromise between the drop-type equilibrium and an attached equilibrium, obviously possible in the square domain.] The circular form of the forming drop supports our theoretical prediction of the drop stability with respect to azimuthal perturbations (Sec. V B). Also, the final (equilibrium) pressure agrees with the drop radius and is predicted quite accurately by the initial conditions.

In a separate simulation (not shown) we organized competition between a slab and a drop. We found that the slab wins. As for numerical simulations of the statistics of a large number of drops, this problem requires special study, and we did not attempt to address it in the present work.

Therefore we were able to reproduce numerically both types of large-scale equilibria predicted by our theory, and verified the stability analysis based on the super-reduced equations. Also, we observed background-mediated competition between "drops" (Ostwald ripening).

VIII. SUMMARY AND DISCUSSION

We have considered the front-curvature effects in the radiative segregation of a confined isotropic thermally bistable plasma. We assumed that the characteristic dimensions of the plasma are much larger than the conductive Field length, but much smaller than the acoustic Field length. This double inequality has made it possible to consistently reduce the full fluid dynamic set of equations for the problem and advance significantly in its analysis.

The front-curvature effects become dominant in the final stage of the dynamics, when the radiative segregation has already been established, the plasma pressure is close to the area-rule value P_*, and the interface motion slows down (see AMS). Then, on the characteristic time scale τ_2, which is proportional to the square of the size of a typical pattern, the curvature effects lead to smoothing of patterns and simplification of their form. The time scale τ_2 is much longer than the time scale τ_1 of the pressure relaxation, which was obtained in the one-dimensional theory of AMS. We have found that the possible types of equilibrium patterns are determined by the condition of a constant sum of the two principal curvatures of their surfaces, showing somewhat unexpected similarity to the classical problem of equilibrium of weightless capillary surfaces. Therefore the simplest individual equilibrium clouds or voids in this system are perfect slabs and spheres, two and three dimensional. We analyzed the stability of these objects with respect to various types of perturbations. We have found that small perturbations of the perfect shape of the equilibrium patterns are damped out. On the other hand, we have discovered an instability of a single spherical cloud (which we call a drop) with respect to purely radial perturbations. We have determined the minimum radius of a stable equilibrium drop. Smaller drops either shrink and disappear or expand until they reach a new, stable equilibrium. Also, we have studied background-mediated competition (Ostwald ripening) in an ensemble of drops. Larger drops always thrive at the expense of the smaller drops, and only the largest drop can finally survive. We found a one-parameter family of "universal" self-similar distribution functions of the clouds with respect to their sizes and corresponding power law time dependences of the pressure mismatch, cloud density, and average cloud radius. It is important that solving the self-similar prob-

lem alone does not provide any selection rule for the parameter β characterizing the family of solutions, so that other considerations (initial conditions and stability arguments) must be invoked. Also, it should be stressed that the self-similar solutions represent an intermediate asymptotics of the dynamics, as finally only the largest cloud survives.

Numerical simulations performed with the reduced model [with the Euler equation replaced by its simplified version (122)] have confirmed many of the predictions of our theory. In addition, we have found that the two simple types of segregated equilibria predicted analytically (slab and drop) can be reached from a variety of initial conditions, so that these objects have extensive basins of attraction in the parameter space.

The original motivation behind the studies of the radiative condensation instability and related segregation processes in optically thin plasmas was to explain the strong inhomogeneities observed in many astrophysical plasmas (such as interstellar and intergalactic clouds and voids, and solar prominences) [1–4] and, more recently, radiative condensations in laboratory plasmas [5]. We have found that a variety of stable, strongly segregated equilibria is indeed possible and attainable in confined plasmas (in contrast to isobaric plasmas, where the final state is usually uniform). Of course, the simple "perfect" objects, which we have found to be in stable equilibrium, cannot explain the frequently observed complexity in the geometric shapes of interstellar clouds and voids [1,17]. Some of the observed complexity might be related to earlier, more violent stages of the dynamics, long before any equilibrium is reached. Indeed, the evaporation fronts' instability of the Darrieus-Landau type, that we consider in Appendix A, can lead to much more complicated (even fractal) shapes. Finally, however, the pressure must approach the area-rule value, and the curvature effects will smooth and simplify the patterns, so that a later stage of the dynamics must be of the type considered in the main body of our paper.

Obviously, more complicated patterns might also appear, if one relaxed the assumptions of isotropy of the plasma motions and heat conduction (both of which are quite unrealistic in view of the complicated magnetic fields permeating the interstellar plasma [17]). Other effects that we neglected (gravity, rotation, ionization-recombination dynamics, etc.) will also influence both the possible equilibria and the relaxation towards them. Now that a reasonably good understanding of the basic multidimensional problem of radiative segregation has been achieved, all these questions are worth studying.

ACKNOWLEDGMENTS

We acknowledge very useful discussions with M. Marder and A. Vilenkin on Ostwald ripening. This work was supported by the Israel Academy of Sciences and Humanities (I.A.) and, in part, by the Russian Fund for Fundamental Research (R.F.F.I.) and by a Soros Foundation grant from the American Physical Society (P.S.).

APPENDIX A: DEFORMATION INSTABILITY OF EVAPORATION FRONTS

We have seen that the characteristic duration τ_2 of the late, curvature-controlled stage of the dynamics is proportional to the square of the pattern dimensions. In this stage, the pressure mismatch is already small, $|P - P_*| \sim \langle \mathcal{K} \rangle \ll 1$, and the front motion slows down significantly. Earlier stages of the dynamics correspond to much larger $|P - P_*|$ and are characterized by faster front motions. These motions (evaporation and condensation fronts) were considered in many works (see Refs. [18,19,10,12]) in the one-dimensional geometry. Indeed, when $|P - P_*| \gg \langle \mathcal{K} \rangle$, the front motions can be treated as almost planar. However, a traveling planar interface can in general be unstable with respect to small deformations of its shape, which should be described in the three-dimensional theory. We found this stability problem to be quite similar to the well known hydrodynamical stability problem for a laminar flame propagation which was investigated in the pioneering works by Darrieus, Landau, and Markstein (see Refs. [32,47–49]). These works predict instability for sufficiently long perturbation wavelengths [the so called Darrieus-Landau (DL) instability]. At short wavelengths, the instability is suppressed by the Markstein effect, related to the perturbation-induced front curvature. The similarity between our problem and that of the DL instability becomes clear when one notices that the unperturbed state in both cases consists in a relatively slow (subacoustic) heat and mass flow through a hydrodynamic discontinuity. The main difference between the two problems is the following. In the laminar flame stability problem, the sign of the material flux through the front j_n is unique (and, in our notation, positive), while in our problem it can be either positive or negative, depending on the sign of the mismatch $P - P_*$. In the following we develop a linear stability theory for moving condensation or evaporation fronts. We assume that the dimensions of the system are infinite, so that the pressure mismatch $P - P_*$ is constant (the corresponding criterion will be checked *a posteriori*).

Let us consider an unperturbed planar front, which is located at the plane $x = 0$ of a Cartesian coordinate system, moving together with the front. A half-space $x > 0$, indexed by D, is assumed to be downstream, and a half-space $x < 0$, indexed by U, is upstream. Indices U and D will also be used for various physical quantities in the U and D regions, respectively. Depending on the sign of $P - P_*$, there are two cases. In the first one $P > P_*$, phase 1 is downstream, phase 2 is upstream, and $j_n < 0$. In the second $P < P_*$, phase 2 is downstream, phase 1 is upstream, and $j_n > 0$. Therefore we can write the unperturbed normal vector $\mathbf{n}$ (see Sec. III) as $(\operatorname{sgn} j_n, 0, 0)$. Other unperturbed values are the following: $c_n = 0$; $v_x/u = \text{const} \equiv j = |j_n| = g|P - P_*|$ (the mass flux across the front in the downstream direction); $v_{i\,n} = j u_i(P) \equiv v_i$; $\mathbf{v}_{i\,t} = 0$ (the index i stands for D or U); $\mathcal{K} = 0$; and $\mathbf{e}_t = (0, \operatorname{sgn} j_n, 0)$ (the unit tangential vector).

Let the function $F(x, y, z, t) = x - \zeta(y, z, t) = 0$ describe a (weakly) perturbed position of the front. As the

unperturbed state is the stationary one and possesses translational and axial symmetries, the dependence of all physical quantities upon (y, z, t) can be chosen proportional to $\exp(qt + ik_y y)$. Denote these linear perturbations (differences between the perturbed and unperturbed quantities) by $'$. Then

$$\mathbf{n}' = (0, -ik_y\zeta, 0)\,\mathrm{sgn}\, j_n\ , \quad \mathbf{e}'_t = (ik_y\zeta, 0, 0)\,\mathrm{sgn}\, j_n\ ,$$

$$v'_{i\ n} = v'_{i\ x}|_{x=0}\,\mathrm{sgn}\, j_n\ ,$$

$$v'_{i\ t} \equiv \mathbf{v}'_i|_{x=0}\mathbf{e}_t + \mathbf{v}_i|_{x=0}\mathbf{e}'_t = (ik_y v_i\zeta + v'_{i\ y}|_{x=0})\,\mathrm{sgn}\, j_n\ ,$$

$$c'_n = q\zeta\,\mathrm{sgn}\, j_n\ ,$$

$$\mathcal{K}' = k_y^2\zeta\,\mathrm{sgn}\, j_n \quad \text{and} \quad j'_n = fk_y^2\zeta\,\mathrm{sgn}\, j_n$$

[the expression for j'_n is obtained from Eq. (49)]. Linearized forms of the matching conditions (42)–(44) are

$$v'_{D\ x} = q\zeta + fu_D k_y^2\zeta, \tag{A1}$$

$$v'_{U\ x} = q\zeta + fu_U k_y^2\zeta, \tag{A2}$$

$$ik_y v_U\zeta + v'_{U\ y} = ik_y v_D\zeta + v'_{D\ y}, \tag{A3}$$

$$\tilde{p}'_U + 2f|j_n|u_U k_y^2\zeta = \tilde{p}'_D + 2f|j_n|u_D k_y^2\zeta. \tag{A4}$$

Linearization of Eqs. (39) and (40) yields

$$\mathrm{div}\,\mathbf{v}'_i = 0, \tag{A5}$$

$$q\mathbf{v}'_i + v_i\frac{\partial}{\partial x}\mathbf{v}'_i = -u_i\frac{\partial\tilde{p}'}{\partial x}\mathbf{e}_x - iu_i k_y\tilde{p}'\mathbf{e}_y \tag{A6}$$

for the regions Ω_U and Ω_D. Here $i = U, D$ or $1, 2$. Equations (A5) and (A6) have the following general solution:

$$\begin{aligned} v'_{i\ x} = {} & A_i\exp(qt + |k_y|x + ik_y y) \\ & + B_i\exp(qt - |k_y|x + ik_y y) \\ & + C_i\exp(qt - qx/v_i + ik_y y), \end{aligned} \tag{A7}$$

$$\begin{aligned} v'_{i\ y} = {} & i\frac{k_y}{|k_y|}A_i\exp(qt + |k_y|x + ik_y y) \\ & - i\frac{k_y}{|k_y|}B_i\exp(qt - |k_y|x + ik_y y) \\ & - i\frac{q}{k_y v_i}C_i\exp(qt - qx/v_i + ik_y y), \end{aligned} \tag{A8}$$

$$\begin{aligned} \tilde{p}'_i = {} & -\frac{1}{u_i|k_y|}(|k_y|v_i + q)A_i\exp(qt + |k_y|x + ik_y y) \\ & - \frac{1}{u_i|k_y|}(|k_y|v_i - q)B_i\exp(qt - |k_y|x + ik_y y), \end{aligned} \tag{A9}$$

where A_i, B_i, and C_i, are arbitrary constants. Since $\tilde{p}'$ must vanish at $|x| \to \infty$, and curl $\mathbf{v} = \mathbf{0}$ in the upstream half-space, i.e., $x > 0$ [50], we obtain

$$\begin{aligned} v'_{D\ x} = {} & B\exp(qt - |k_y|x + ik_y y) \\ & + C\exp(qt - qx/v_i + ik_y y), \end{aligned} \tag{A10}$$

$$v'_{Ux} = A\exp(qt + |k_y|x + ik_y y), \tag{A11}$$

$$\begin{aligned} v'_{D\ y} = {} & -i\frac{k_y}{|k_y|}B\exp(qt - |k_y|x + ik_y y) \\ & - i\frac{q}{k_y v_D}C\exp(qt - qx/v_i + ik_y y), \end{aligned} \tag{A12}$$

$$v'_{U\ y} = i\frac{k_y}{|k_y|}A\exp(qt + |k_y|x + ik_y y), \tag{A13}$$

$$\tilde{p}'_D = \frac{1}{u_D|k_y|}(q - |k_y|v_D)B\exp(qt - |k_y|x + ik_y y), \tag{A14}$$

$$\tilde{p}'_U = -\frac{1}{u_U|k_y|}(q + |k_y|v_U)A\exp(qt + |k_y|x + ik_y y). \tag{A15}$$

Substituting Eqs. (A10)–(A15) in Eqs. (A1)–(A4), we obtain a linear homogeneous system of four equations with respect to the four unknown parameters A, B, C, and ζ. The solvability condition of this system gives a cubic equation with respect to q. One root of this equation, $q = |k_y|v_D$, describes, however, a trivial solution $\mathbf{v}' = \tilde{p}' = \zeta = 0$. Therefore we are left with the following quadratic dispersion relation:

$$\begin{aligned} q^2 + 2q\frac{k|j_n|u_1u_2}{u_1 + u_2}\left(1 + \frac{fk}{|j_n|}\right) + {} & k^2 j_n^2\frac{u_U - u_D}{u_U + u_D}u_D u_U \\ & + 2fk^3|j_n|\frac{u_D^2 u_U}{u_U + u_D} = 0, \end{aligned} \tag{A16}$$

where $k \equiv |k_y|$. The real part of one of its roots is always negative [51], while the other root,

$$\begin{aligned} q = -\frac{kju_1u_2}{u_1 + u_2} \times \Bigg[& 1 + \frac{fk}{j} \\ & - \sqrt{1 + \frac{f^2k^2}{j^2} + \left(\frac{u_2}{u_1} - \frac{u_1}{u_2}\right)\mathrm{sgn}\, j_n - 2\frac{fk}{j}\frac{u_D}{u_U}}\Bigg], \end{aligned} \tag{A17}$$

can have a positive real part, which corresponds to instability. Indeed, one can see that evaporation fronts [for which always $j_n = g(P_* - P) > 0$] are unstable ($\mathrm{Re}\, q > 0$), if the perturbation wavelength is sufficiently large:

$$0 < k < k_0 = \frac{1}{2}\frac{j_n}{f}\frac{u_1}{u_2}\frac{u_2 - u_1}{u_2 + u_1}. \tag{A18}$$

The maximum growth rate can be estimated as $q \sim u_{1,2}j_n^2/f \sim (P - P_*)^2$. It goes to zero with the pressure mismatch. When $P > P_*$, one has $\mathrm{Re}\, q < 0$, so that condensation fronts are always stable.

Expression (A17) is very similar to the growth rate of the DL instability. In particular, condition (A18) corresponds to the curvature stabilization of the DL instability (Markstein effect). It is essential that $f > 0$ in our problem, so that no analogs of the thermodiffusive flame instability [49] (or Mullins-Sekerka instability in solidification [52]) appear.

Now we can check our assumption that the pressure difference $P - P_*$ remains constant. This assumption is valid if the characteristic growth rate of the DL-type instability is much higher than the typical inverse time τ_1^{-1} of the pressure relaxation towards P_*. Assuming that neither u_1 nor u_2 introduces large or small parameters, we can write this inequality as $|P - P_*| \gg 1/\langle L \rangle$, where $\langle L \rangle$ is the typical size of patterns. Correspondingly, an *opposite* inequality is a necessary criterion for the validity of the stability analyses presented in the main body of the paper.

Nonlinear effects of the DL instability in flame front dynamics were considered in a number of works, starting from the original work of Landau [53]. The instability tends to increase the front's area, which leads to front acceleration. In the extreme case, the front surface can even become fractal [49]. Presently, there are attempts to calculate the fractal dimension of the flame front surface [54,55]. All these questions are relevant in the dynamics of evaporation fronts as well; however, they are beyond the scope of this paper.

Let us briefly summarize the results of this Appendix. Condensation fronts are always stable with respect to the deformation (DL-type) instability; therefore the curvature-dominated dynamics for such patterns, considered in the main body of the paper, is unchallenged. In contrast, the dynamics of evaporation fronts can be very complicated at an earlier stage of the evolution. However, even in this case the latest stage of the dynamics will be dominated by curvature, as the pressure finally approaches P_* and the growth rate of the DL-type instability goes to zero.

APPENDIX B: NONSPHERICAL DROPS AND BUBBLES

In this Appendix we present a formal derivation of Eq. (33) with $\mathcal{K}$ defined in Eq. (36) for "smooth" large-scale interfaces. Let us define a new quantity $\overline{R}$, which represents the minimum of the following quantities: the absolute values of the principal curvature radii of the interfaces, distances between different interfaces, distances between different "remote" parts of the same interface, and distances between the interfaces and the boundaries of the box. We assume that $\overline{R} \gg 1$. Let us consider Eq. (27). Neglecting effects exponentially small with respect to $\overline{R}^{-1}$ essentially means that we consider, instead of exact solutions, some "quasisolutions," which, according to definition, satisfy the following relation at $\overline{R} \to \infty$:

$$\nabla \cdot (u^\alpha \nabla u) - P_{eq}^{-\alpha} \lambda(u, P_{eq}) = O_e \ , \qquad \text{(B1)}$$

where O_e goes to zero faster than any power of $1/\overline{R}$ at $\overline{R} \to \infty$. In other words, we are looking for smooth large-scale solutions, describing *quasiequilibrium* states of the bistable plasma. In fact, such a state evolves in time. However, this evolution is *exponentially* slow, which keeps these solutions in the state of "quasiequilibria."

As $\overline{R} \to \infty$, the nonlinear eigenvalue problem for Eq. (B1) with the boundary condition (25) can be treated perturbatively. As usual, the zero approximation is provided by the planar eigenvalue problem

$$\frac{d}{dx} u^\alpha \frac{d}{dx} u - P_{eq}^{-\alpha} \lambda(u, P_{eq}) = 0 \ , \quad \left. \frac{d}{dx} u \right|_{\pm\infty} = 0 \ . \qquad \text{(B2)}$$

Let Σ be a smooth surface, approximating the interface, dividing the phases 1 and 2, and let $|s(\mathbf{x})|$ be the distance between any point $\mathbf{x}$ and the interface. We shall take s positive if $\mathbf{x}$ is located at the side corresponding to the phase 2, and negative in the opposite case. Let $A(\mathbf{x}) \in \Sigma$ be the corresponding point on the surface Σ, closest to the point $\mathbf{x}$. We can consider the set of pairs (A, s) as a local coordinate system in a (sufficiently large) region, close to the surface Σ. [Outside this region, we can put $u(P_{eq}, \mathbf{x}) = u_{1,2}(P_{eq})$.] Also, we can choose $\mathbf{n} = \nabla s$ as the "smooth" unit vector field, entering Eq. (36). Let us look for a solution of Eq. (B1) in the following form:

$$u(P_{eq}, \mathbf{x}) = u_{(0)}(P_*, s) + u_{(1)}(A, s) \ , \qquad \text{(B3)}$$

where $u_{(0)}(P_*, s)$ is the solution of Eq. (B2) with the boundary conditions $u_{(0)}(P_*, \pm\infty) = u_{2,1}(P_*)$, corresponding to the eigenvalue $P = P_*$ (see, e.g., AMS), $u_{(1)} = O(1/\overline{R})$, and $P_{eq} - P_* = O(1/\overline{R})$ as $\overline{R} \to \infty$. The "longitudinal" component of the gradient of $u_{(1)}$ is $\partial u_{(1)}/\partial s = O(1/\overline{R})$ for $|s| \sim 1$, and exponentially small for $\overline{R} \gg |s| \gg 1$. The "transverse" component of the gradient of $u(P_{eq}, \mathbf{x})$ is the following: $(\mathbf{n} \times \nabla u) \equiv (\mathbf{n} \times \nabla u_{(1)}) \sim O(1/\overline{R}^2)$, that is, of the next order of smallness. Therefore s and A can be considered as "fast" and "slow" variables, respectively. Let us substitute Eq. (B3) into Eq. (B1). Being interested in the first-order correction to P_{eq}, we arrive at the following equation:

$$\frac{1}{1+\alpha} \left(\frac{\partial}{\partial s} \right)^2 u^{1+\alpha} + \mathcal{K} u^\alpha \frac{\partial}{\partial s} u + P_{eq}^{-\alpha} \lambda(u, P_*)$$

$$+ P_*^{-\alpha} \mu(u)(P_{eq} - P_*) = O(1/\overline{R}^2) \ , \qquad \text{(B4)}$$

where $\mathcal{K} = (\operatorname{div} \mathbf{n})\big|_{s=0}$. The origin of the second term in the left hand side of Eq. (B4) (this term is of the order of $1/\overline{R}$) can be seen from the following calculation:

$$\nabla \cdot \{ [u_{(0)}(s)]^\alpha \nabla u_{(0)}(s) \}$$

$$= \nabla \cdot \left[u_{(0)}^\alpha \mathbf{n} \left(\frac{\partial}{\partial s} \right) u_{(0)} \right]$$

$$= \frac{\partial}{\partial s} \left(u_{(0)}^\alpha \frac{\partial}{\partial s} u_{(0)} \right) + [u_{(0)}(s)]^\alpha (\operatorname{div} \mathbf{n}) \frac{\partial}{\partial s} u_{(0)} \ , \qquad \text{(B5)}$$

where $u_{(0)} \equiv u_{(0)}(P_*, s)$. Multiplying Eq. (B5) by $u^\alpha (\partial u/\partial s)$ and integrating the resulting equation along those "field lines" of the field $\mathbf{n}$ which cross the surface Σ, we obtain

$$\mathcal{K}\int_{-\infty}^{+\infty} u_{(0)}^{2\alpha}\left(\frac{du_{(0)}}{dx}\right)^2 dx$$

$$+P_*^{-\alpha}(P_{eq}-P_*)\int_{-\infty}^{+\infty} u_{(0)}^{\alpha}\mu(u_{(0)})\frac{du_{(0)}}{dx}\,dx$$

$$= O(1/\overline{R}^2)\ . \quad \text{(B6)}$$

To arrive at Eq. (B6), we have used the exponential smallness of $\partial u/\partial s$ at large distances from the surface Σ. Also, we have replaced (under the integral) the functions u and $\partial u/\partial s$ by their zero-order values $u_{(0)}$ and $\partial u_{(0)}/\partial s$, respectively, in the two terms which are of the first order of smallness with respect to $1/\overline{R}$. Finally, since $u_{(0)}(x)$ is the solution of the eigenvalue problem (B2) with $P = P_*$, a zero-order term vanished due to the area rule (30).

Equation (B6) leads directly to Eq. (37) with $\mathcal{K} = (\mathrm{div}\,\mathbf{n})\big|_{s=0} \equiv 1/R_1 + 1/R_2$ (the last identity is well known in differential geometry; see, e.g., [29]). One can see that Eq. (33) is an expansion of some "exact" formula in the powers of $1/\overline{R}$. Also, as in many other eigenvalue problems, finding the first-order correction to the eigenvalue P_{eq} proves to be much easier than finding the corresponding correction to the eigenfunction itself.

[1] L. Spitzer, *Physical Processes in the Interstellar Medium* (Wiley, New York, 1978); S. A. Kaplan and S. B. Pikel'ner, *Physics of the Interstellar Medium* (Nauka, Moscow, 1979) (in Russian).

[2] G. B. Field, Astrophys. J. **142**, 531 (1965).

[3] K. Davidson, Astrophys. J. **171**, 213 (1972).

[4] E. Tandberg-Hanssen, *Solar Prominences* (Reidel, Dordrecht, 1974); *Dynamics and Structure of Quiescent Solar Prominences*, edited by E. R. Priest, Astrophysics and Space Science Library Vol. 150 (Kluwer Academic Publishers, Dordrecht, 1989).

[5] J. L. Terry, E. S. Marmar, and S. M. Wolfe, Bull. Am. Phys. Soc. **26**, 886 (1981); B. Lipshultz, J. Nucl. Mater. **145**, 15 (1987).

[6] R. S. Pease, Proc. R. Soc. London Ser. B **70**, 11 (1957); S. I. Braginskii, Zh. Eksp. Teor. Fiz. **33**, 645 (1957) [Sov. Phys. JETP **6**, 494 (1958)]; J. D. Lawson, J. Nucl. Energy C **1**, 31 (1959); V.V. Neudachin and P.V. Sasorov, Nucl. Fusion **31**, 1053 (1991).

[7] B. I. Meerson and P. V. Sasorov, Zh. Eksp. Teor. Fiz. **92**, 531 (1987) [Sov. Phys. JETP **65**, 300 (1987)].

[8] P. V. Sasorov, Pis'ma Astron. Zh. **14**, 306 (1988) [Sov. Astron. Lett. **14**, 129 (1988)].

[9] B. Meerson, Astrophys. J. **347**, 1012 (1989).

[10] A. M. Dimits and B. Meerson, Phys. Fluids B **3**, 1420 (1991).

[11] C. Elphick, O. Regev, and N. Shaviv, Astrophys. J. **392**, 106 (1992).

[12] I. Aranson, B. Meerson, and P. V. Sasorov, Phys. Rev. E **47**, 4337 (1993).

[13] B. Meerson, E. R. Priest, and C. D. C. Steele, Geophys. Astrophys. Fluid Dynamics **71**, 243 (1993).

[14] B. Meerson, C. D. C. Steele, A. M. Milne, and E. R. Priest, Phys. Fluids B **5**, 3417 (1993).

[15] G. Van Hoven, L. Sparks, and D. D. Schnack, Astrophys. J. **317**, L91 (1987); J. T. Karpen, S. K. Antiochos, J. M. Picone, and R. B. Dahlburg, *ibid.* **338**, 493 (1989); L. Sparks, G. Van Hoven, and D. D. Schnack, *ibid.* **353**, 297 (1990).

[16] R. J. Bray, L. E. Cram, C. J. Durrant, and R. E. Loughhead, *Plasma Loops in the Solar Corona*, Cambridge Astrophysics Series Vol. 18 (Cambridge University Press, Cambridge, England, 1991).

[17] H. Scheffler and H. Elsässer, *Physics of the Galaxy and Interstellar Medium* (Springer-Verlag, Berlin, 1987).

[18] Ya. B. Zel'dovich and S. B. Pikel'ner, Zh. Eksp. Teor. Fiz. **56**, 310 (1969) [Sov. Phys. JETP **29**, 170 (1969)].

[19] M. V. Penston and F. E. Brown, Mon. Not. R. Astron. Soc. **150**, 373 (1970).

[20] A.V. Nedospasov and V. D. Khait, *Oscillations and Instabilities in Low-Temperature Plasmas* (Nauka, Moscow, 1979), p. 116 (in Russian).

[21] L. Pismen, Chem. Eng. Sci. **34**, 563 (1979).

[22] V. V. Barelko, V. M. Beybutyan, Yu. V. Volodin, and Ya. B. Zeldovich, Dokl. Akad. Nauk. SSSR **257**, 339 (1981) [Sov. Phys. Dokl. **26**, 335 (1981)].

[23] U. Middya, M. Sheintuch, M. D. Graham, and D. Luss, Physica D **63**, 393 (1993).

[24] Our results on the possible forms of segregated equilibria (see Sec. III) will be valid in the general, unsimplified case.

[25] M. C. Begelman and C. F. McKee, Astrophys. J. **358**, 375 (1990).

[26] P. Fife, *Mathematical Aspects of Reacting and Diffusing Systems*, Lecture Notes in Biomathematics Vol. 28 (Springer-Verlag, New York, 1979).

[27] H. Lamb, *Hydrodynamics* (Cambridge University Press, Cambridge, England, 1932).

[28] A. S. Mikhailov, *Foundations of Synergetics I. Distributed Active Systems* (Springer-Verlag, Berlin, 1990), p. 27.

[29] A. Gray, *Modern Differential Geometry of Curves and Surfaces* (CRC Press, Boca Raton, 1993).

[30] Notice the striking similarity between this problem and a classical problem of equilibrium of capillary surfaces without gravity [31]. The similarity is quite unexpected, as no "conventional" surface tension is present in this problem.

[31] R. Finn, *Equilibrium Capillary Surfaces* (Springer-Verlag, New York, 1986).

[32] L. D. Landau and E. M. Lifshitz, *Fluid Mechanics* (Pergamon Press, Oxford, 1959).

[33] It should be remembered that Eqs. (90) and (91) and Eqs. (95) and (96) are not valid for too large drops which are of the order of the size of the system.

[34] I. M. Lifshitz and V. V. Slezov, Zh. Eksp. Teor. Fiz. **35**, 479 (1958) [Sov. Phys. JETP **8**, 331 (1959)].

[35] C. Wagner, Z. Electrochem. **65**, 581 (1961).

[36] Of course, the finally surviving drop must correspond to the stable part of the single-drop equilibria line, shown

in Fig. 2. Otherwise, no drop will survive.
[37] W. Ostwald, Z. Phys. Chem. **34**, 495 (1900).
[38] V. V. Slezov and V. V. Sagalovich, Usp. Fiz. Nauk **151**, 67 (1987) [Sov. Phys. Usp. **30**, 23 (1987)].
[39] M. Marder, Phys. Rev. A **36**, 858 (1987).
[40] L. C. Brown, Acta Metall. Mater. **40**, 1293 (1992).
[41] M. K. Chen and P. W. Voorhees, Modelling Simul. Mater. Sci. Eng. **1**, 591 (1993).
[42] J. H. Yao, K. R. Elder, H. Guo, and M. Grant, Phys. Rev. B **47**, 14 110 (1993).
[43] Obviously, τ can be replaced by $\tau - \tau_0$ with any τ_0, which is nothing but the choice of the reference time.
[44] V. V. Slezov, J. Phys. Chem. Solids **39**, 367 (1978).
[45] Notice that, though in the case of $\beta > 5\sqrt{2}/4$ the solution (121) diverges at $\xi = \xi_1$, it is still normalizable on the interval $(0, \xi_1)$.
[46] L. C. Brown, Acta Metall. **37**, 71 (1989); Scr. Metall. Mater. **24**, 963 (1990); **24**, 2231 (1990).
[47] Ya. B. Zeldovich, G. I. Barenblatt, V. B. Librovich, and G. M. Makhviladze, *The Mathematical Theory of Combustion and Explosions* (Consultants Bureau, New York, 1985).
[48] P. Pelcé, *Dynamics of Curved Fronts* (Academic Press, Boston, 1988).
[49] A. Liñán and F. A. Williams, *Fundamental Aspects of Combustion* (Oxford University Press, New York, 1993).
[50] Suppose that the initial vorticity is zero. Then, owing to Eq. (41), curl **v** will be nonzero only for the fluid elements which passed across the front, that is, downstream.
[51] Notice that in the limit of $j \to 0$ this root yields the damping rate (78) for the static front deformations.
[52] W. Kurz and D. J. Fisher, *Fundamentals of Solidification* (Trans Tech Publications, Aedermannsdorf, 1992).
[53] L. D. Landau, Acta Physicochim. URSS **19**, 77 (1944) (see also a reprinted version in [48]).
[54] L. Filyand, G. I. Sivashinsky, and M. L. Frankel, Physica D **72**, 110 (1994).
[55] S.I. Blinnikov and P.V. Sasorov (unpublished).

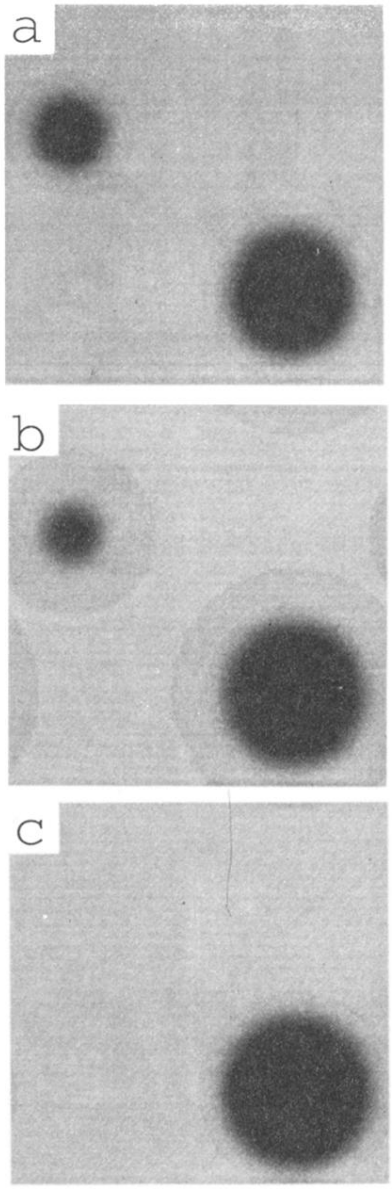

FIG. 3. Background-mediated competition between two drops, studied numerically. We started with two drops ($u = u_1$) in the "vapor" ($u = u_2$) for the initial pressure 1.2. The dimensions of the system are 60×60. Shown are the specific volume contours at $t = 5$ (a), 45 (b), and 100 (c).

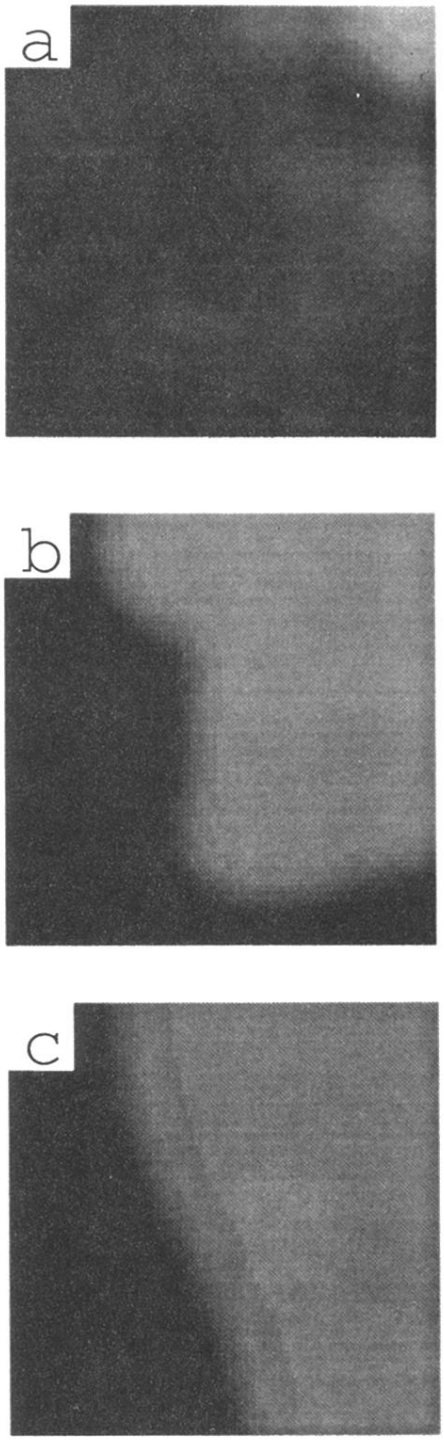

FIG. 5. Slab-type equilibrium, developing from a broad-band noise. We started from a small-amplitude multimode perturbation of u around $u_0 = 0.9$. The initial pressure is 1.0; the dimensions of the system are 40×40. Shown are the specific volume contours at $t = 10$ (a), 20 (b), and 250 (c).

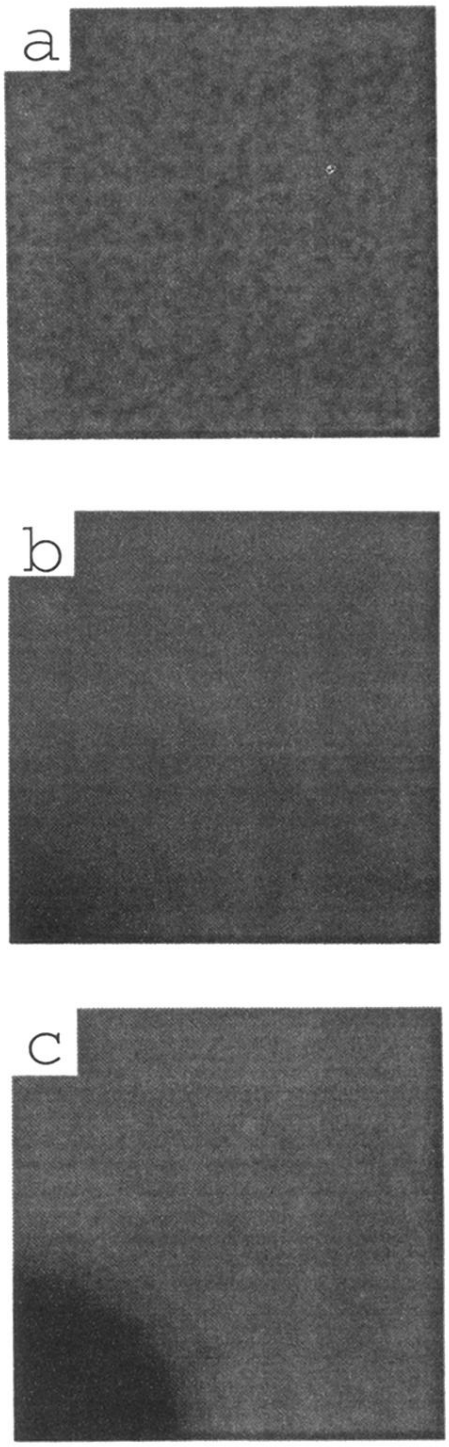

FIG. 7. Drop-type equilibrium, developing from a broad-band noise. We started from a small-amplitude multimode perturbation of u around $u_0 = 1.4$. The initial pressure is 1.2, the dimensions of the system are 35×35. Shown are the specific volume contours at $t = 0$ (a), 20 (b), and 180 (c).